Solvation and the Excited-State Tautomerization of 7-Azaindole and 1-Azacarbazole: Computer Simulations in Water and Alcohol Solvents

S. Mente and M. Maroncelli*

Department of Chemistry, The Pennsylvania State University, University Park, Pennsylvania 16802

Received: January 13, 1998; In Final Form: March 19, 1998

Computer simulations are performed in order to investigate the role hydroxylic solvents play in catalyzing the excited-state tautomerization of 7-azaindole (7-AI) and 1-azacarbazole (1-AC). Classical Monte Carlo and molecular dynamics methods are used to test the idea that reaction rates in these systems are controlled primarily by the fraction of solutes that are "correctly" solvated. Assuming that correct solvation involves formation of a cyclic 1:1 solute−solvent complex, reactive fractions are computed for a series of eight hydroxylic solvents: methanol, ethanol, 1-propanol, 2,2,2-trifluoroethanol, 2-propanol, *tert*-butyl alcohol, ethylene glycol, and water. In all cases the reactive fractions so calculated are small (<2%) and are of the correct magnitude to account for the relatively slow reaction observed in neat solvents. The underlying cause for these small reactive populations can be rationalized on the basis of the weak hydrogen bonds afforded by a cyclic arrangement. In nearly all cases these fractions correlate nicely with the observed reaction rates, thereby validating the basic picture of the solvent involvement in these reactions developed on the basis of experimental studies.

I. Introduction

7-Azaindole ("7-AI") and 1-Azacarbazole ("1-AC"; Scheme 1) are representatives of a class of molecules that undergo rapid excited-state tautomerization in the presence of suitable hydrogen-bonding partners. These molecules have attracted considerable attention for a number of reasons. In the earliest work, excited-state tautomerization in 7-AI dimers was examined as a model for radiation-induced processes in DNA base pairs.[1] In dimers, tautomerization is believed to be effected by a double proton switch between the two components of the dimer (Scheme 1b), one of which is electronically excited and the other of which is in the ground state. Reaction in both 7-AI and 1-AC dimers occurs in a few picoseconds in room-temperature solution[2−4] and nearly this quickly at the low temperatures achieved in supersonic expansion.[5,6] Studies of 1-AC and 7-AI complexed to single molecules of various carboxylic acids, amides, and lactams[4,7,8] have also shown very rapid reaction, especially in cases where the complexing partner acts as a catalyst (i.e. is chemically unchanged) in the process. In addition to studies of isolated complexes, a number of workers have investigated the excited-state tautomerization of 7-AI[9−18] and 1-AC[19−21] in bulk alcohol and water solvents. These systems present a striking contrast to the former cases in that in bulk alcohols and water the reaction is found to occur hundreds to thousands of times more slowly at room temperature. In addition, in bulk solvents the reaction is strongly activated such that decreasing the temperature to near 200 K results in unobservably slow reaction.

The mechanism of the solvent involvement in the tautomerization of 7-AI in bulk alcohols and especially in bulk water has been the subject of considerable discussion. Virtually all workers postulate that formation of a 1:1 cyclically bonded 7-AI−ROH complex of the sort shown in Scheme 1c is a prerequisite to reaction. The difference between reaction rates in dilute solution and bulk protic solvents is generally attributed to difficulty of forming such reactive structures in bulk solution.[22] The kinetics is most simply described by the two-step mechanism shown in Figure 1a. The second step of this mechanism, which involves the actual proton transfer, is assumed to be rapid (k_{PT}^{-1} < 5 ps)) by analogy to reactions in isolated complexes. Prior to excitation, most 7-AI molecules are solvated in a manner not conducive to reaction. Little if any prompt reaction observed, and the reaction rate is largely dictated by the initial, solvent-reorganization step. Two limits can be envisioned for how this solvent-reorganization step affects reaction, and both limits have been used for interpretation of experimental data. In one limit the solvent-reorganization step can be assumed to be rate-limiting such that the observed rate constant for reaction is roughly k_1. The opposite limit is reached when solvent equilibration is rapid relative to k_{PT}. In

SCHEME 1

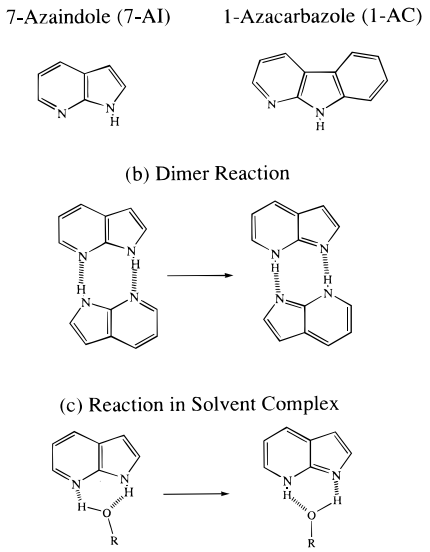

S1089-5639(98)00771-3 CCC: $15.00
Published on Web 05/08/1998

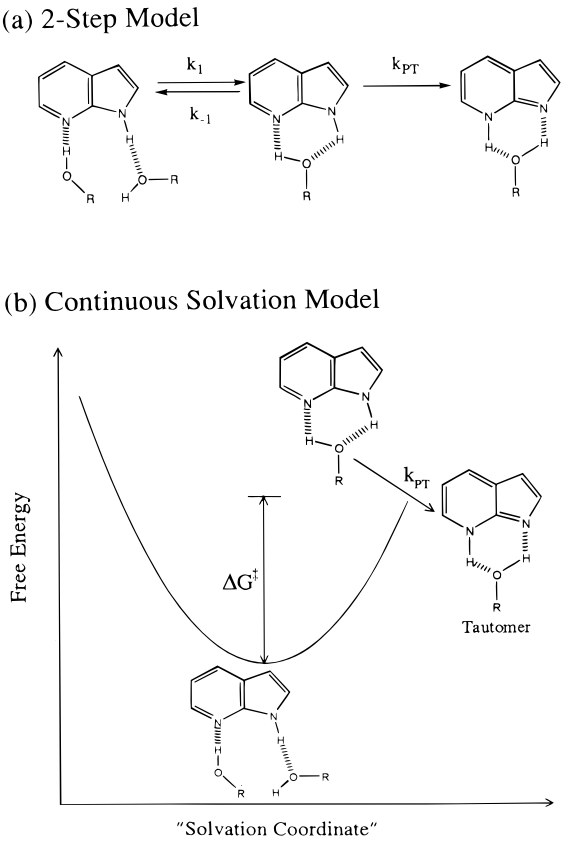

Figure 1. Two views of the mechanism of the solvent-catalyzed tautomerization of 7-AI in alcohol solvents.

this second limit the observed reaction rate has nothing to do with solvent dynamics but is controlled by an equilibrium solvation property, the equilibrium constant $K_{solv} = k_1/k_{-1}$. Evidence in favor of both the dynamical[10,11,13] and the static[12,21] role for the solvent has found roughly equal representation in the experimental literature on the 7-AI reaction.

In recent studies of the 1-AC reaction, we have argued that the equilibrium solvation effects dominate in controlling both of these reactions.[21] The description that emerged from this experimental work is illustrated in Figure 1b. It is essentially the same as the equilibrium model discussed above except that the discrete solvation step is replaced by a more realistic continuous solvation potential. The observed rate of reaction is expressed in the manner of transition-state theory (TST) as[23]

$$k_{obs} = k_{PT} f^{\ddagger} = k_{PT} \exp(-\Delta G^{\ddagger}/(k_B T)) \qquad (1.1)$$

In this expression $f^{\ddagger}$ is the fraction of molecules correctly solvated for reaction and $\Delta G^{\ddagger}$ is their free energy relative to the more prevalent nonreactive forms. All of the features observed for 7-AI and 1-AC in bulk alcohol solvents can be rationalized by assuming that all isotope sensitivity comes from a rapid proton-transfer process, $k_{PT} > (5\ \text{ps})^{-1}$, which is, to a reasonable first approximation, both temperature- and solvent-independent and which is about 5-fold larger in 7-AI than in 1-AC. Variations in the reaction rates observed in different alcohol solvents and the temperature dependence of these rates come primarily from differences in the equilibrium fraction of correctly solvated species, $f^{\ddagger}$. The solvent dependence of this fraction is approximately the same in 7-AI and 1-AC, and at least in alkyl alcohols this dependence is well correlated with various measures of solvent hydrogen-bonding ability.[21]

The model portrayed in Figure 1b provides a consistent explanation of the behavior observed in all alcohol solvents and in water. However, Petrich and co-workers[15] argue that the situation in water is qualitatively different from that in alcohol solvents. They interpret their observations of the 7-AI reaction as indicating that only a small fraction (<20%) of the 7-AI in a room-temperature aqueous solution are correctly solvated to tautomerize relatively rapidly (in 40−100 ps). Most (>80%) of the solutes are envisioned to be in a state of solvation that "blocks" tautomerization for times longer than the ∼1 ns lifetime of the excited state. Chou et al.[18] share the viewpoint that the emission characteristics of 7-AI in water reflect the inability of 7-AI to tautomerize as a result of the different solvation structure in water compared with that in alcohol solvents. Our interpretation of the emission spectra of 7-AI in water is that the observed lifetime of 800 ps in fact represents the reaction time of *all* of the 7-AI solutes.[15] Similar observations can be made with respect to 1-AC in water. Although the reaction times are slower than in alcohols, we envision the mechanism and the solvation states involved to be much the same in water as in alcohol solvents.[21]

The various interpretations of how solvent is involved in the tautomerization of 7-AI and 1-AC in water and alcohols reflect differing conceptions of the structures and dynamics of solvation in these systems. Although schematic pictures and considerable discussion of solvation structure are available in the literature, no attempt to quantitatively model these systems has been made to date.[24] The present paper represents such an attempt.

We have performed Monte Carlo (and to a much lesser extent molecular dynamics) simulations of 7-AI and 1-AC in alcohol and water solvents. Using what we believe to be realistic intermolecular potentials, we explore the structure and dynamics of solvation in these systems in an effort to determine whether the existing interpretations of the solvent participation in these reactions are reasonable. The simulations undertaken here are purely classical. If one adopts the perspective of Figure 1b, the relative rates of reaction in different solvents should only reflect the equilibrium reactive fractions $f^{\ddagger}$ in these solvents. Thus, the proton-transfer step, which would require consideration of quantal aspects of the reaction, need not be explicitly considered. The bulk of this paper concerns Monte Carlo simulations used to test the extent to which variations in solvation structure (i.e., $f^{\ddagger}$) are sufficient to understand the variations observed in the experimental rates. We have simulated a total of eight different hydroxylic solvents with either 7-AI or 1-AC as the solute. The results show that, despite the uncertainties in intermolecular potentials, the solvation structures simulated in both aqueous and alcoholic solutions are semiquantitatively consistent with the mechanistic description discussed in connection with Figure 1b.

The outline of the remainder of the paper is as follows. Section II describes the details of the simulation methods and the intermolecular potential functions employed. The results are then presented in section III, which is divided into five parts. Part A contrasts the nature of the hydrogen bonding present in dilute solution (where reaction is assumed to be rapid) and bulk methanol in order to display the qualitative nature of the solvent effect on reaction. Part B concerns the possible role of solvent dynamics in controlling the reaction rates. Here, we employ molecular dynamics simulations in methanol and water to show that the TST perspective of eq 1.1 is a valid approximation. These results are also used to discuss the improbability of long-lived or "blocked" solvation states in these solvents. In Part C we discuss quantitative measures for the reactive fractions $f^{\ddagger}$

and how these fractions are influenced by uncertainties in the charges used to model the interactions between the solute and solvents. The main results of this study are contained in section III.D, where we describe the nature of the solvation of 7-AI in the eight solvents, methanol, ethanol, 1-propanol, 2,2,2-trifluroethanol (TFE), 2-propanol, *tert*-butyl alcohol, ethylene glycol, and water, and how differences in solvation lead to differences in the reactive fractions simulated. Finally, in Part E we consider two additional aspects of the simulations that can be compared with experimental results: the temperature and solute dependence of the reactive fractions in methanol and water. A summary of the main results of this work along with ideas for future directions is provided in section IV. There is also an Appendix to this paper, in which we examine some features of the new set of solvent potentials used in this work in comparison with more standard potentials and experimental data.

II. Simulation Methods

A. Methodology. Most of the simulations reported here were Monte Carlo calculations carried out using the "BOSS" molecular simulation program developed by Jorgensen.[25] Simulations were performed in the isothermal−isobaric (*NPT*) ensemble at a temperature of 25 °C and 1 atm pressure. Each simulation system consisted of 104 (or 252 in the case of water) solvent molecules and 1 solute in a cubic cell, with periodic boundary conditions. Tests with larger system sizes showed that these relatively small samples were adequate to display bulklike behavior for the properties of interest here.

Solvent−solvent interactions were spherically truncated at cutoff distances r_c based on oxygen−oxygen atom distances. A solute−solvent cutoff r_{sc} was applied such that if any solute atom−solvent oxygen atom distance was less than r_{sc}, the interaction between the entire solute and solvent molecule was included. In both cases these cutoffs were taken to be approximately one-half of the periodic cell length. New configurations were generated by randomly selecting a molecule and performing random moves of translational, (external) rotational, and internal rotational coordinates. The range of each type of move was chosen to yield acceptance ratios of approximately 0.4 for new configurations. These ranges were 0.2 Å for translations, 20° for external rotations, and 15° for internal rotations. Attempts to change the volume of the system (with a range of ±150 Å^3) were made every 700 configurations, and all intermolecular distances were scaled accordingly.

All simulations were started from a random configuration that had been previously equilibrated from a liquidlike arrangement of solvent molecules for a period of at least 2×10^7 configurations. Energies and densities were monitored in order to ensure adequate convergence within the equilibration period. After equilibration, simulations for a given system were performed in five or more segments of 2×10^7 configurations each in order to compute statistical uncertainties. The uncertainty values reported here are ±1 standard deviation of the mean of the averages obtained from individual runs.

Both Boltzmann and non-Boltzmann sampling methods were employed in this work.[27] Non-Boltzmann sampling was required in order to quantitatively determine equilibrium constants for cyclic complex formation because of the fact that in a Boltzmann-sampled Metropolis scheme the "cyclic" region of phase space is only infrequently visited. In the sampling method adopted here acceptance of moves that are uphill in energy is biased by a weighing factor dependent on two key solute−solvent hydrogen-bonding distance parameters, R_{NH} and R_{HO} discussed in more detail in section III (see Figure 3).

$$P(R_{NH}, R_{HO}) = \frac{w(R_{NH}, R_{HO})_{new}}{w(R_{NH}, R_{HO})_{old}} \exp(-\beta \Delta U) \qquad (2.1)$$

In this equation, $P(R_{NH}, R_{HO})$ is the probability of a move's acceptance, β is the inverse of the absolute temperature multiplied by Boltzmann's constant, ΔU is the difference in potential energy between old and new configurations, and $w(R_{NH}, R_{HO})$ refers to a biasing function whose value depends on the intermolecular distances of the solute−solvent pair. For the latter we chose a "Gaussian cliff" shape:[28]

$$w = \begin{cases} 1 + a_1\{\exp(-a_2[(R_{NH} - R^0_{NH})^2 + (R_{HO} - R^0_{HO})^2]\}^2 & R_{NH} \geq R^0_{NH};\ R_{HO} \geq R^0_{HO} \\ 1 + a_1 & R_{NH} < R^0_{NH};\ R_{HO} < R^0_{HO} \end{cases} \qquad (2.2)$$

This weighting function is only applied for moves involving the particular solvent molecule closest to the solute (defined in terms of R_{NH}). The distances R^0_{NH} and R^0_{HO} were both set to 2.0 Å, and the height ($20 < a_1 < 200$) and width parameters ($1 < a_2 < 3$ Å^{-1}) of the "cliff" were chosen for each solvent to best sample both the "cyclic" region and the noncyclic regions of phase space visited by a Boltzmann-weighted simulation. The latter condition is necessary in order to use a pair of simulations (one biased and one unbiased) to compute the desired equilibrium population densities ρ_0 from the density observed in the biased simulation ρ_w via the relation

$$\rho_0(R_{NH}, R_{HO}) = \frac{\rho_w(R_{NH}, R_{HO})/w(R_{NH}, R_{HO})}{\langle 1/w(R_{NH}, R_{HO})\rangle_w} \qquad (2.3)$$

The results obtained for ρ_0 using this scheme were compared with those found using a regular Boltzmann sampled simulation in the region where both simulations were sampled adequately to ensure that the parameters were chosen reasonably.

In addition to the Monte Carlo calculations, which comprise the majority of this paper's content, molecular dynamics simulations were also performed for two systems: 7-AI in methanol and 7-AI in water. These simulations were performed in the *NVE* ensemble with cubic periodic boundary conditions using programs described in ref 29. The number of molecules was the same as in the MC runs, and the density and average kinetic energy were chosen to correspond as closely as possible to the (*NVT*) Monte Carlo simulations.

B. Intermolecular Potential Functions. *1. General Form.* Molecules were represented as collections of interaction sites with intermolecular interactions modeled via site−site Lennard-Jones plus Coulomb terms,

$$v_{ij} = 4\epsilon_{ij}\left[\left(\frac{\sigma_{ij}}{r_{ij}}\right)^{12} - \left(\frac{\sigma_{ij}}{r_{ij}}\right)^{6}\right] + \frac{q_i q_j}{r_{ij}} \qquad (2.4)$$

The Lennard-Jones parameters between unlike atoms were determined from the like-atom parameters (provided below) using the mixing rules $\sigma_{ij} = (\sigma_{ii}\sigma_{jj})^{1/2}$ and $\epsilon_{ij} = (\epsilon_{ij}\epsilon_{jj})^{1/2}$. In general, each atom within a molecule corresponded to an individual site, with the exception of the CH_n groups of the alcoholic solvents, which were taken as single units centered on carbon. (In the dilute solution studies the cyclohexane supporting solvent was also modeled as a single Lennard-Jones site.)

TABLE 1: Solute Properties and Potential Parameters

A. Lennard Jones Parameters[a]

atom type	σ (Å)	ϵ (kcal/mol)
C	3.5	0.08
N	3.25	0.17
H (−C)	2.5	0.05
H (−N)	0	0

B. Electrical Properties Calculated for the Ground and Low-Lying Excited States

state	calculation[b]	E^c (kJ/mol)	μ (D)	$\theta_\mu{}^d$ (deg)	$q_{N5}{}^e$ (au)	$q_{N6}{}^e$ (au)	$q_H{}^e$ (au)
			7-Azaindole				
S_0	6-31G*	(0)	1.67	33	−0.57	−0.67	+0.41
S_0	AM1/CI	(0)	1.53	22	−0.44	−0.36	+0.40
S_1	AM1/CI	330 (412)	2.72	15	−0.44	−0.38	+0.41
S_2	AM1/CI	377	4.20	8	−0.38	−0.44	+0.39
			1-Azacarbazole				
S_0	6-31G*	(0)	1.15	56	−0.81	−0.71	+0.46
S_0	AM1/CI	(0)	0.82	53	−0.70	−0.40	+0.45
S_1	AM1/CI	320 (361)	1.50	20	−0.61	−0.38	+0.45
S_2	AM1/CI	345	1.36	8	−0.69	−0.44	+0.46

[a] Parameters optimized for nucleotide bases in ref 31. [b] See text and ref 35 for details. [c] Values in parentheses are experimental gas-phase values estimated from the data in ref 41. [d] Dipole orientation as defined in Figure 2. [e] ESP-fit charges on the nitrogen atoms of the five- and six-membered rings ("q_{N5}" and "q_{N6}") and the transferring H atom (q_H).

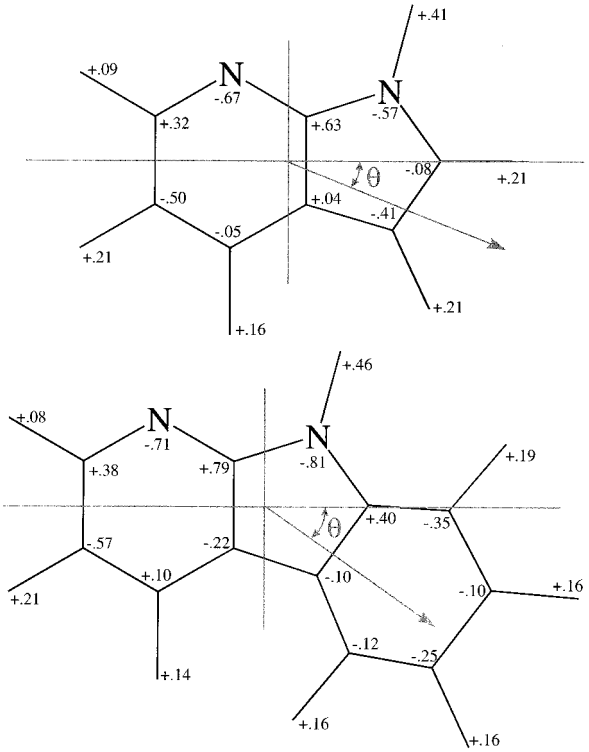

Figure 2. Charges used in modeling the solutes 7-AI and 1-AC. These charges are from ESP fits to the HF 6-31G* ab initio wave functions of the solutes (for geometries optimized using the MNDO semiempirical method).

2. Solute Models. The solutes 7-AI and 1-AC, were both represented by rigid all-atom models. The geometries were those optimized for the ground states calculated at the restricted Hartree−Fock level using the semiempirical MNDO Hamiltonian.[30] The Lennard-Jones parameters were taken from the OPLS potential functions for nucleotide bases[31] and are listed in Table 1A. The charges used in the modeling were from electrostatic potential fits of the ground-state HF wave functions generated using a 6-31G* basis set.[32] These charges are shown in Figure 2. A complete set of charges and coordinates for the solutes is available in the Supporting Information.

Some comment should be made regarding the use of ground-state charges to model solvation effects in these excited-state reactions. This choice is dictated by our inability to accurately calculate the excited-state charge distributions of these molecules. On the basis of considerable prior work[33] as well as results with 7-AI and 1-AC,[34] we trust that the ESP-fit charges calculated at the 6-31G* provide good representations of electrical interactions between the ground states of these solutes and other molecules. However, it is not possible to calculate excited-state properties of such large molecules using either ab initio or semiempirical methods with comparable accuracy. Thus, we rely on the ground-state charges and assume that, at least at the solute "active sites" for reaction and hydrogen bonding, they do not differ much between the ground and excited states. Some evidence in support of this assumption is provided by the semiempirical calculations shown in Table 1B. Here, we compare some electrical characteristics of the solutes in different electronic states derived from AM1-CI calculations.[35] As can be seen from this table, there is very little difference between the charges that should determine solute−solvent hydrogen bonding in the ground and lowest-lying excited states of either solute.

3. Solvent Models. Two different solvent representations, based on the OPLS models of Jorgensen,[37−39] were employed here. Parameters are listed in Table 2. Both representations use the standard bond lengths and bond angles of the OPLS set, which are described in ref 38. These parameters are kept fixed during the simulations, but torsional motion is included using the torsional potentials also taken from the OPLS parametrization.[38] The difference between the two types of solvent representation involves only the charges on the H and O atoms of the hydroxyl group and the C atom to which it is attached ("C_O" in Table 2). The first set comprises what we will term the "ab initio" solvents, so-called because charges were obtained from ESP fits to the charge distribution generated from geometry-optimized 6-31G* calculations. Solvents in the second set are the true OPLS models, in which these charges were optimized for liquid-state properties by Jorgensen and coworkers.[38,39] The latter solvents maintain the same charges for the three atoms mentioned above in all alcohols. In reality, over the set of alcohols examined here, one observes significant

TABLE 2: Parameters of the Solvent Models[a]

solvent	atom/group	q (au)	σ (Å)	ϵ (kcal/mol)
	Ab Initio Solvents			
methanol	−O	−0.674	3.070	0.170
	−H	+0.424	0.0	0.0
	$-CH_3$	+0.250	3.775	0.207
ethanol	−O	−0.710	3.070	0.170
	−H	+0.417	0.0	0.0
	$-CH_2$	+0.348	3.905	0.118
	$-CH_3$	−0.045	3.775	0.207
1-propanol	−O	−0.717	3.07	0.170
	−H	+0.421	0.0	0.0
	$-CH_2$	+0.311	3.905	0.118
	$-CH_2$	+0.077	3.905	0.118
	$-CH_3$	−0.093	3.775	0.207
trifluoroethanol	−O	−0.611	3.07	0.170
	−H	+0.427	0.0	0.0
	$-CH_2$	+0.230	3.905	0.118
	$-C(F)_3$	+0.569	3.80	0.1094
	−F	−0.205	3.50	0.061
2-propanol	−O	−0.756	3.070	0.170
	−H	+0.430	0.0	0.0
	−CH	+0.665	3.850	0.080
	$-CH_3$	−0.170	3.910	0.160
tert-butyl alcohol	−O	−0.770	3.07	3.170
	−H	+0.428	0.0	0.0
	$-C_O$	+0.856	3.80	0.05
	$-CH_3$	−0.168	3.96	0.145
ethylene glycol	−O	−0.667	3.07	0.170
	−H	+0.423	0.0	0.0
	$-CH_2$	+0.244	3.905	0.118
water	−O	−0.790	3.1506	0.1521
	−H	+0.395	0.0	0.0
acetic acid	−O	−0.684	3.0	0.17
	−H	+0.455	0.0	0.0
	−C	+0.908	3.75	0.105
	$-CH_3$	−0.042	3.91	0.16
	=O	−0.636	2.96	0.21
cyclohexane	C_6H_{12}	0.000	5.65	0.590
	OPLS Solvents			
alcohols	−O	−0.700	3.070	0.170
	−H	+0.435	0.0	0.0
	$-C_O$	+0.265	3.775	0.207
TIP3P water	−O	−0.834	3.1506	0.1521
	−H	+0.417	0.0	0.0
SPC water	−O	−0.820	3.1656	0.1554
	−H	+0.410	0.0	0.0

[a] Other than the charge parameters for the ab initio solvents, which were obtained from ESP fits to the 6-31G* wave functions, all but the F atom parameters are from the OPLS set described in refs 37−39. Parameters for the CF_3 group were adapted from ref 40.

variations in the ESP-fit−ab initio charges at these sites. Since such variations might be significant in determining the reactive fractions of interest, we chose the ab initio solvents as our primary working models despite their slightly poorer performance in reproducing properties of the pure liquid solvents (see the Appendix for details).

III. Results and Discussion

A. General Behavior. Isolated Complexes versus Bulk Solvents. One of the clearest indications that solvation structure is a primary determinant of reaction rates in 7-AI− and 1-AC− alcohol systems is the contrast between the rates observed in bulk alcohol solvents and dilute solution. In the latter case, when only isolated 1:1 complexes are formed, reaction occurs hundreds to thousands of times faster than in bulk alcohol solvents. We therefore begin with a comparison of the differences in the solvation structures simulated under these two conditions. We consider 1:1 and 1:2 complexes of 7-AI with methanol and other hydrogen-bonding partners in dilute solution. To mimic a nonassociating background solvent of the sort employed in experiment, we use a single-site Lennard-Jones model of "cyclohexane" (Table 2). Representative results are shown in Figure 3.

In Figure 3 and later figures we display the solvation structure in a given system using two-dimensional plots of the relative frequency of occurrence of a pair of distances R_{NH} and R_{HO}. These two distances specify the hydrogen bonding between the solvent and the two "active sites" for reaction, the pyridyl N atom and the transferring H atom, as indicated in Figure 3. When only a single methanol molecule is present in the simulation ("7-AI−MeOH"), the configurations observed are predominantly structures in which both distances R_{NH} and R_{HO} are approximately 2 Å. These distances imply that most of the time the lone alcohol molecule is simultaneously hydrogen-bonded to both active sites of the solute, as illustrated in Scheme 2. This structure is presumably what is required for reaction, and in keeping with past nomenclature, we label it as "cyclic". Note that the distribution of the 7-AI−MeOH complex shows it to be reasonably "loose", with a substantial fraction of the population occurring with R_{NH} distances that are larger than nominal hydrogen-bonding distances (∼2.5 Å). Thus, whereas the H_U-O_V hydrogen bond is intact nearly all of the time, the N_U-H_V hydrogen bond is frequently broken in the cyclic complex. (Here and in what follows the subscripts "U" and "V" denote atoms of the sol*u*te and sol*v*ent, respectively.) This situation in the methanol 1:1 complex should be contrasted with that of the 1:1 7-AI−acetic acid complex, also shown in Figure 3. In this complex, short hydrogen-bonding distances to the acid H(−O) and O(=C) atoms are found essentially 100% of the time.

When more than a single alcohol molecule is present, there is a marked change in the type of solvation observed. As illustrated by the 7-AI−$(MeOH)_2$ data in Figure 3, two peaks rather than one appear in the population distribution. These peaks occur with one of the distance parameters being ∼2 Å (hydrogen-bonded) and the other being distinctly greater than 2 Å, spanning a range from about 2.5 to 4 Å. This change reflects the loss of cyclic complexes and the dominance of the second type of structure shown in Scheme 2. This class of configurations, which we designate as "eight-membered ring" structures is one in which two solvent molecules are singly hydrogen-bonded to the solute and also hydrogen-bonded to one another. It has been speculated that this type of arrangement may facilitate tautomerization via a three-proton shuttling mechanism in systems such as 7-hydroxyqunoline, in which the active sites are too widely separated to be bridged by a single solvent molecule.[42] However, the results presented below suggest that such a three-proton shuttling mechanism does not play a significant role in the 7-AI or 1-AC reactions. Note that the peaks in the distribution of the 2:1 complex are much narrower than in the 1:1 case, which reflects the more rigid hydrogen bonding present in this case.

The situation in bulk methanol appears outwardly similar to that existing in the 1:2 complex. The addition of many more possible hydrogen-bonding partners results in even fewer occurrences of "cyclic" solvation. However, careful inspection of Figure 3 also reveals that the long R_{NH} and R_{HO} distances are in fact larger than in the 1:2 complex. The peaks are also broader. These differences reflect the fact that the predominant mode of solvation in bulk methanol does not involve the eight-membered ring structure but rather "neighbor-bonded" structures of the sort illustrated in Scheme 2. In bulk solution the two

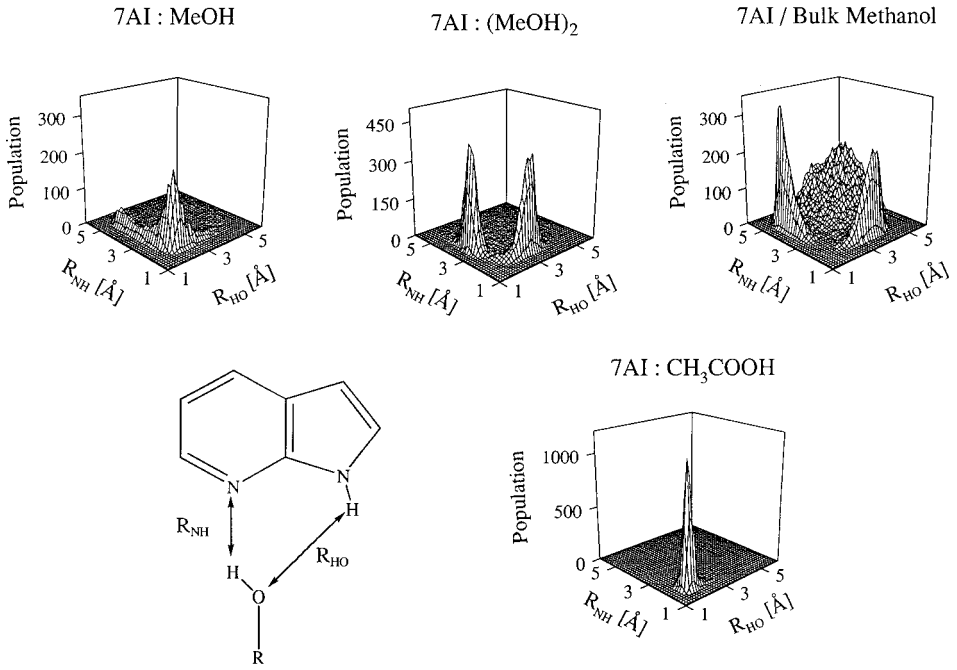

Figure 3. Hydrogen-bonding distance distributions (see text) observed in simulations of 7-AI in cyclohexane containing either one or two molecules of methanol, one molecule of acetic acid, and in bulk methanol solvent. In the case of acetic acid, the R_{HO} distance plotted is the distance from the carbonyl oxygen of the acetic acid to the H(N) atom of 7-AI.

SCHEME 2

Hydrogen Bonding Structures

Reactive Configuration Unreactive Configurations

"Cyclic" "8-Membered Ring" "Neighbor Bonded"

alcohol molecules hydrogen-bonded to the solute mainly form hydrogen bonds to other neighboring solvent molecules rather than to one another. (As will be discussed later, in methanol one only observes the eight-membered ring structure to occur ~7% of the time.)

These examples, taken from simulations of methanol with 7-AI, are typical of the behavior observed with 7-AI or 1-AC in other alcohol solvents. The general conclusions one draws from such simulations are in keeping with what has been postulated on the basis of experimental results. When 7-AI or 1-AC can form 1:1 complexes with alcohols or other appropriate hydrogen-bonding partners, it usually forms cyclically hydrogen-bonded structures that facilitate rapid reaction. But formation of "correct" cyclic structures is severely inhibited in bulk alcohol solvents. In bulk alcohols, or indeed whenever more than a single alcohol molecule is available there is a strong preference for two different solvent molecules to hydrogen-bond to the solute, a situation that appears to prohibit proton transfer.

The reason that cyclic forms are disfavored in bulk alcohols is simply a matter of the poor hydrogen bonds afforded by the cyclic structure. Figure 4 serves to illustrate this point. Here, we have plotted distributions of the molecular pair interaction energies corresponding to the systems in Figure 3. The average interaction energy between 7-AI and methanol in the isolated 1:1 complex, where the cyclic structure predominates, is −27.5 kJ/mol. Dividing this value by the number of hydrogen bonds

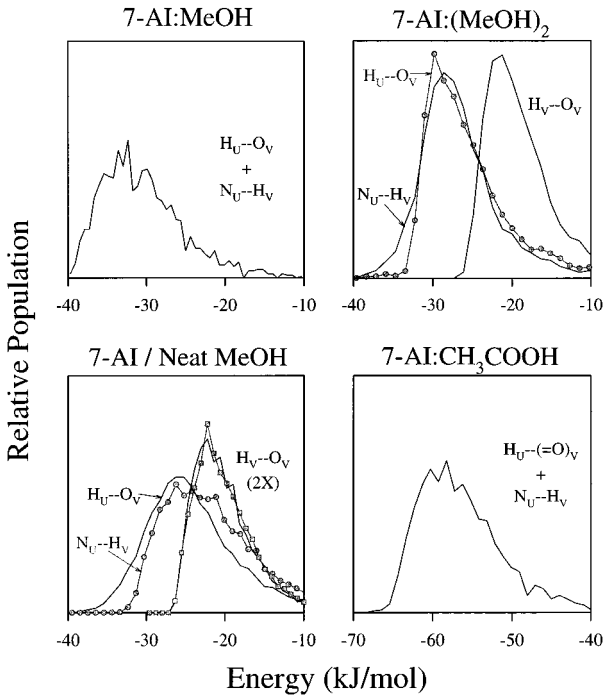

Figure 4. Pair energy distributions observed in the same systems as in Figure 3. These energies are the total interaction energies between pairs of molecules in the solvation structures shown in Scheme 2. Indicated on each panel are the particular hydrogen-bonding interactions involved in each pair interaction, with N_U and H_U denoting the sol*u*te active sites and H_V and O_V sol*v*ent sites. In the case of the 1:1 complexes, the single molecular pair interaction incorporates two hydrogen-bonding interactions, while for the 1:2 complex and bulk solvent there are three and four pairs involved, respectively (see Scheme 2).

in the structure yields ~14 kJ/mol per hydrogen bond—a relatively small value indicative of weak hydrogen bonding.[43] In the 7-AI−$(MeOH)_2$ complex, where the eight-membered ring structure predominates, the three solute−solvent and solvent−solvent interactions amount to ~25 kJ/mol per hydrogen bond,

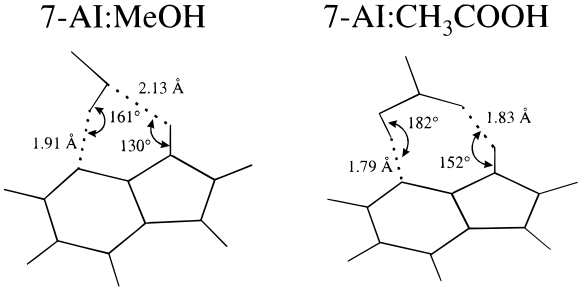

Figure 5. Structures of the energy-minimized (gas-phase) 7-AI−methanol and 7-AI−acetic acid complexes. These structures were derived with the classical potential energy functions used in the simulation.

a much more respectable number. A similar value is also found in the "neighbor-bonded" structure characteristic of bulk methanol solvation, ∼24 kJ/mol per hydrogen bond. Thus, as soon as more than a single alcohol molecule is available for hydrogen bonding with the solute, it is energetically advantageous to break up the cyclic structure in favor of these other noncyclic structures. As will be discussed later, the free energy penalty paid for reaching the cyclic form is essentially just this energy cost of trading strong for weak hydrogen bonds.

Hydrogen bonds are relatively weak in cyclic 7-AI alcohol complexes mainly as a result of the poor geometric fit that a single O−H bond from an alcohol molecule makes with the 7-AI "active site". This fact is evident when one compares the energetics and geometries of the 1:1 acetic acid and alcohol complexes. Energy-minimized structures of these complexes derived from the simulation potentials are shown in Figure 5. (Ab initio calculations of these complexes yield similar structures[4,44,45].) With acetic acid and geometrically comparable molecules such as amides,[4] the 1:1 complex is "tighter" (as shown by the distributions in Figure 3) and the average hydrogen-bonding energy much larger, ∼28 kJ/mol primarily because the complexing agent's geometry allows for more nearly linear hydrogen bonds to both solute sites.

The two solutes 7-AI and 1-AC should be nearly identical in this regard (see part F), and variation of the identity of the alcohol also makes little difference to this observation. However, it is useful to recognize that a single alcohol molecule can provide strong cyclic bonding in some situations. A recently reported case is the solute "DPC" illustrated in Figure 6. In this case, the additional separation of the active sites leads to a good geometric fit and strong cyclic hydrogen bonding. As shown in the top panel of Figure 6, the population distribution of DPC in bulk methanol is such that there is essentially always an alcohol molecule cyclically bonded to one of the two active sites. In contrast to the 7-AI and 1-AC reactions, this solute was observed to undergo unresolvably rapid (τ_{rxn} < 30 ps) tautomerization in methanol at room temperature.[46]

B. Possible Dynamical Solvent Effects on the Reaction Rate. The interpretation of the 7-AI and 1-AC reactions described in the Introduction assumes that the solvent's influence is primarily a static rather than a dynamic effect. That is, differences in the reaction rates observed in different solvents are viewed as resulting from variations in the equilibrium free energy change between reactive and nonreactive forms and not from the dynamics of interconversion between these forms. To verify this assumption, we have performed molecular dynamics simulations in two bulk solvents: methanol and water.

To assess the importance of dynamical solvent effects, we employ the "stable-states picture" ("SSP") of Hynes and coworkers.[47] Within the SSP formalism the net rate constant k_{net}

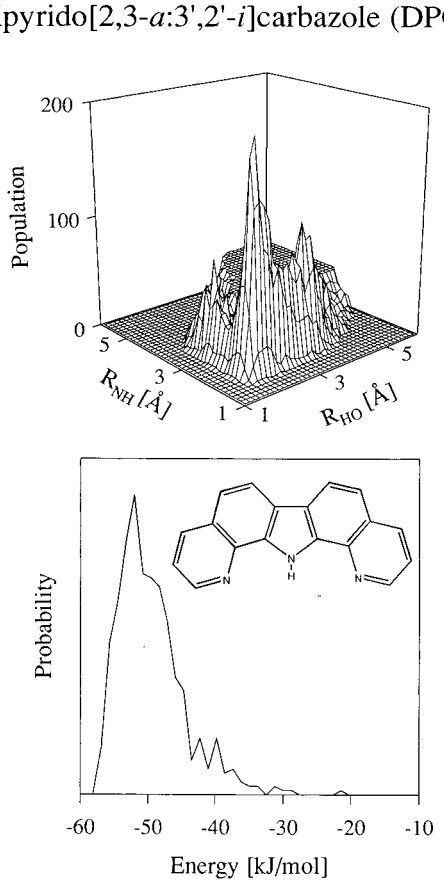

Figure 6. Hydrogen-bonding distance and pair energy distributions simulated for the DPC solute in bulk methanol. The hydrogen-bonding distance plot is cut off at distances beyond 3 Å to enhance the visibility of the peak corresponding to the solute−solvent hydrogen bonding.

observed for an irreversible activated process is given by

$$k_{net}^{-1} = k_i^{-1} + k_D^{-1} \tag{3.1}$$

where k_i is the rate constant associated with the barrier crossing when internal equilibrium is maintained within the reactant region and k_D is the rate constant associated with producing this reactant equilibrium. In the present context k_i represents the reaction rate (k_{obs}) of eq 1.1, which implicitly assumes that solvent dynamics are rapid enough that $f^{\ddagger}$ represents the equilibrium fraction of reactive species. The constant k_D then represents the rate of the hydrogen-bonding rearrangements that interconvert reactive and nonreactive forms. From eq 3.1 one sees that for $k_D \gg k_i$ the solvent dynamics becomes irrelevant and $k_{net} = k_i$, as has been assumed in eq 1.1. Thus, the equilibrium assumption can be tested by comparing k_D with $k_i = k_{PT} f^{\ddagger}$. According to the SSP, k_D is given by[48]

$$k_D^{-1} = \frac{1}{f^{\ddagger}} \int_0^{\infty} dt \{P(\ddagger, \ddagger; t) - f^{\ddagger}\} \tag{3.2}$$

where $P(\ddagger, \ddagger; t)$ is the conditional probability that if the system is in the reactive configuration ("‡") at time zero, it will also be found there at some later time t. Since $f^{\ddagger} \ll 1$ (see below), given the form of eqs 3.2 and 1.1, the comparison to be made here reduces to comparing the "survival time" of the reactive configuration,

$$\tau_{\ddagger} = \int_0^{\infty} dt\, P(\ddagger, \ddagger; t) \tag{3.3}$$

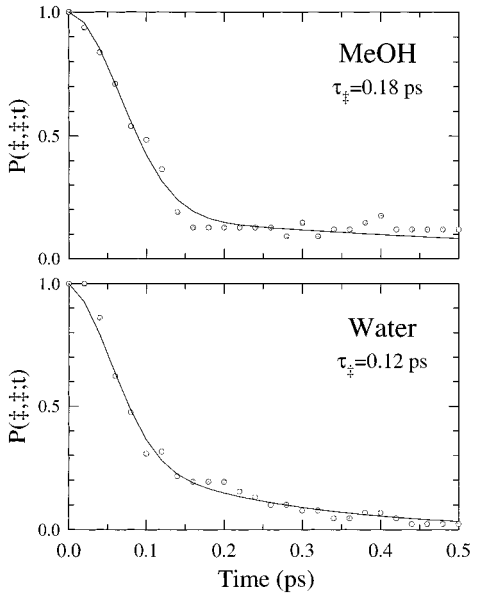

Figure 7. Time-dependent survival probabilities of cyclic structures (R_{NH}, R_{HO} < 2.69 Å) observed in methanol and water. The values of $\tau_{\ddagger}$ are the integrals under these functions.

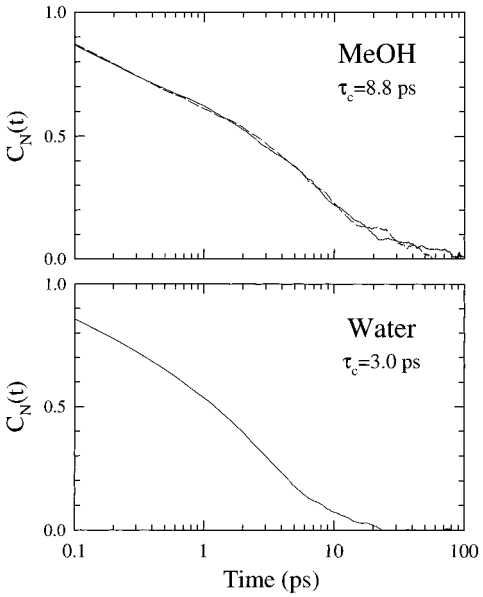

Figure 8. Structural time correlation functions (eq 3.4) in methanol and water. In the methanol case two curves are shown, corresponding to calculations involving spherical regions surrounding the solute active site with radii $R = 5$ (solid) and 6 (dashed) Å. These two regions enclose an average of five and nine solvent molecules, respectively. In the water case the radius was 5 Å and the region contained an average of ∼10 solvent molecules. The values of τ_c noted are the integrals under these functions.

with the intrinsic proton-transfer rate τ_{PT} once the reactive geometry is achieved.

Figure 7 shows the survival probabilities $P(\ddagger, \ddagger, t)$ determined for 7-AI in bulk methanol and water solvents. (How we define a reactive geometry is discussed in detail in the following section; here, we employ the criterion $R_{NH} = R_{HO} = 2.69$ Å.) The plots in Figure 7 were generated from equilibrium molecular dynamics simulations simply by waiting for the system to adopt a reactive geometry and then following its fate forward and backward in time from there. Although the data are somewhat noisy (only 19 occurrences of reactive geometries were observed in methanol and 22 in water), they suffice to show that the survival times for this definition of reactive geometry are in the subpicosecond range. As will be discussed in the following section, the estimated value of τ_{PT} is predicted to be at least 10-fold larger for this same definition of reactive geometry. Other definitions also yield comparable results. In all cases the cyclic geometry is sufficiently unstable in bulk methanol and water such that it not only occurs infrequently but when it does occur it persists for only a very short time.[49] Thus, the assumption that it is a static solvation property ($f^{\ddagger}$) and not the time dependence of solvation that determines the reaction rates appears justified.

In addition to these survival times, it is also of interest to briefly consider other measures of the dynamics of the solute−solvent hydrogen-bonding structure in these systems. We do so mainly in light of conjectures about "blocked" solvation states of 7-AI in alcohol and water solvents. To explain the distinctive spectral features of 7-AI in water, other workers have proposed that although some 7-AI molecules can undergo rapid reaction, a large fraction exist in solvation environments that preclude reaction for times of a nanosecond or more.[15,16,18] Several features of the present simulations make such long-lived solvation states seem unlikely. For example, we find that solvent molecules bound to 7-AI have roughly the same diffusional characteristics as bulk solvent molecules. (Experimentally, water and methanol have approximately the same self-diffusion constant at room temperature, $(2.3-2.4) \times 10^{-5}$ cm^2 s^{-1}.[50]) A molecule of methanol or water hydrogen-bonded to either "active site" of 7-AI is observed to diffuse out of the first solvation shell (i.e., move a distance of ∼3 Å) in a time of 3−5 ps, just as would be expected from these bulk diffusion constants. The lifetime of a solute−solvent hydrogen-bonded pair observed here is comparable to the lifetimes of solvent−solvent hydrogen bonds in the neat liquids.[51]

As another measure of the time scale for structural relaxation, we also examined how long a particular group of solvent molecules maintained "contact" with the solute. By defining a spherical region of radius R surrounding the "active site" for reaction (choosing the origin midway between the N_U and H_U atoms), we monitored the exchange dynamics of molecules within this region via the correlation function

$$C_N(t) \equiv \frac{\langle \sum_i \theta[R - r_i(t)]\theta[R - r_i(0)]\rangle}{\langle \sum_i \theta[R - r_i(t)]\rangle} \qquad (3.4)$$

In this expression θ represents the Heaviside step function and r_i denotes the position of the oxygen atom of solvent molecule i. This correlation function reports on the fraction of the molecules that were originally solvating the active site still remaining in this region after an elapsed time t. Figure 8 shows such $C_N(t)$ functions for 7-AI in methanol and water. For R values encompassing a reasonable number of solvent molecules (5−20), the decay of this function is relatively insensitive to the particular choice of R. (As illustrated in the top panel of Figure 8, one finds nearly identical $C_N(t)$ functions for two choices of R (5.0 and 6.0 Å), which contain an average of five and nine solvent molecules.) As noted in the figure, the correlation times of these correlation functions involving ∼10 solvent molecules are 9 and 3 ps in methanol and water, respectively. By times on the order of 100 ps there is little probability of finding even a single one of the original 10 solvent molecules still solvating the active site of the 7-AI solute. We

also note that there is nothing exceptionally slow about water compared with alcohols such as methanol. To the contrary, the reorganization dynamics in water are considerably faster than the dynamics in methanol and presumably also those in larger alcohols. Thus, if the simulations performed here are at all realistic, it is difficult to envision how "blocked" solvation states could persist for times of about a nanosecond in the 7-AI−water system.

C. Quantitative Estimation of Reactive Fractions and Reaction Rates. Given that the dynamics of the solvation process exert only a minor influence over the rates of these reactions, we now focus exclusively on quantitative estimates of the reactive fraction $f^{\ddagger}$, or equivalently, the free energy change $\Delta G^{\ddagger}$. Doing so requires that we choose a definition of which solvent configurations constitute reactive forms. Although there has been some study of the ground-state reaction path in 1:1 complexes of 7-AI with water and methanol,[45] the choice is not clear-cut. After considering several possible geometric and energetic criteria,[52] we settled on the simplest choice, which is based on the two hydrogen-bonding distances R_{NH} and R_{HO} already discussed. Specifically, we measure the fractional populations $f(R^{\ddagger})$ contained within regions of (R_{NH}, R_{HO}) space defined as ($R_{NH} \leq R^{\ddagger}$, $R_{OH} \leq R^{\ddagger}$) for three different values of $R^{\ddagger}$: 2.19, 2.44, and 2.69 Å. The smallest value, $R^{\ddagger} = 2.19$ Å, corresponds approximately to the distances observed in the minimum energy structures of gas-phase complexes between 7-AI and water or methanol as determined from either ab initio calculations[44,45] or from classical calculations using the simulation potentials (Figure 5). The largest distance, 2.69 Å, is approximately equal to the position of the first minimum in the N_U-H_V and H_U-O_V radial distribution functions, and 2.44 Å is simply an intermediate value.

The fractions so obtained for the systems discussed in part A are listed in Table 3A. These quantitative estimates of the reactive fractions amplify the observations made earlier. Depending on the distance criterion chosen, we find that in 1:1 7-AI−methanol complexes, somewhere between 9 and 40% of the systems are prepared for reaction at any given time. (Reaction in the remaining fraction of the system would also be expected to be rapid, since there is little to prohibit the noncyclic-to-cyclic interconversion in this case.) In 1:1 acetic acid complexes, the much stronger hydrogen bonding present renders $f^{\ddagger} \approx 100\%$ for all three reaction criteria. Compared with these two cases, the fractions estimated for the 1:2 methanol complex are much smaller, <1% for all three choices of $R^{\ddagger}$. These observations are in qualitative accord with experimental observations. However, there are as yet no experimental data yet available that can be quantitatively compared with these dilute solution results.

More direct comparison is available in the case of the bulk alcohols. In neat methanol, and in many other alcohols as we will show shortly, the reactive fractions calculated are in reasonable quantitative agreement with experimental data. Even for the largest value of $R^{\ddagger}$ examined here, the fraction of reactive molecules is quite small, less than 2% in the 7-AI−bulk methanol system. Such a small fraction is consistent with the observation of no noticeable (<5%) prompt reaction in either 7-AI−methanol, 1-AC−methanol, or other bulk alcohol solutions.[12,13,21] The fractions observed are also consistent with the kinetic model described by eq 1.1. By use of the reactive fractions listed in Table 3 and the experimentally observed rate of the 7-AI reaction in bulk methanol, $\tau_{obs} = k_{obs}^{-1} = 124 \pm 30$ ps, an estimate of the time constant of the proton-transfer event can be estimated as

TABLE 3: 7-Azaindole−Methanol Results

A. Isolated Complexes and Bulk Methanol[a]

system	$f^{\ddagger}$(2.19 Å) (10^{-3})	$f^{\ddagger}$(2.44 Å) (10^{-3})	$f^{\ddagger}$(2.69 Å) (10^{-3})
7AI−$(MeOH)_1$	89 ± 11	278 ± 14	412 ± 13
7AI−$(MeOH)_2$	9 ± 3	40 ± 10	92 ± 16
7AI−MeOH	2.5 ± 0.4	9.0 ± 1.3	20 ± 2
7AI−CH_3COOH	923 ± 20	980 ± 15	995 ± 5

B. Solute Charge Variations[b]

(q_N, q_H)	$f^{\ddagger}$(2.19 Å) (10^{-3})	$f^{\ddagger}$(2.44 Å) (10^{-3})	$f^{\ddagger}$(2.69 Å) (10^{-3})
"low q" (−0.57, +0.31)	3.1 ± 0.5	15 ± 2	32 ± 3
"normal" (−0.67, +0.41)	2.5 ± 0.4	9.0 ± 1.3	20 ± 2
"high q" (−0.77, +0.51)	0.39 ± 0.13	1.8 ± 0.3	7.8 ± 0.4

C. Solvent Charge Variations[c]

(q_O)	$f^{\ddagger}$(2.19 Å) (10^{-3})	$f^{\ddagger}$(2.44 Å) (10^{-3})	$f^{\ddagger}$(2.69 Å) (10^{-3})
"low q" (−0.600)	3.5 ± 0.7	17 ± 3	35 ± 5
"normal" (−0.674)	2.5 ± 0.4	9.0 ± 1.3	20 ± 2
"high q" (−0.800)	1.2 ± 1.2	3 ± 2	10 ± 4

[a] Reactive fractions $f(R^{\ddagger})$ are the fractional populations contained within regions ($R_{NH} \leq R^{\ddagger}$, $R_{HO} \leq R^{\ddagger}$), where R_{NH} and R_{HO} are the solute−solvent hydrogen-bonding distances defined in Figure 3. Uncertainties listed are ±1 standard deviation of the mean of 10 subsets of the overall simulation. [b] Charges on the 7-azaindole "active sites" (the pyrrolic N atom and the H−(N) atom) varied as indicated. The solvent is "normal" (ab initio) bulk methanol. [c] Charges on the methanol solvent varied from their "normal" (Gaussian) values by moving the charge from the O atom from the CH_2 united atom to which it is attached.

$$\tau_{PT} = k_{PT}^{-1} = f^{\ddagger}\,\tau_{obs} \tag{3.5}$$

From such a calculation we obtain proton-transfer times ranging from 0.31 ps ($R^{\ddagger} = 2.19$ Å) to 2.5 ps ($R^{\ddagger} = 2.69$ Å). On the basis of the reaction time measured in the 7-AI dimer (~1 ps[2,3]) and the time estimated for the 1-AC−acetic acid complex (0.7 ± 0.2 ps[4]), this range of times nicely brackets the value anticipated for a 1:1 7-AI−MeOH complex. (Given the steep dependence of tunneling probability on distance, the best criterion to choose is probably $R^{\ddagger} = 2.19$ Å, which would predict a value of 0.31 ± 0.09 ps for the proton-transfer event.) Thus, although our incomplete knowledge of the geometry required for reaction and lack of more experimental data on isolated complexes precludes a very precise comparison between experiment and simulation, these results are encouraging. It appears that the hydrogen-bonding equilibria simulated here are at least semiquantitatively consistent with eq 1.1 and the description on which it is based. We will show shortly (part D) that the same can also be said for the other solvents examined here.

However, before discussing values of $f^{\ddagger}$ simulated in different solvents, it is useful to first consider the extent to which these values are sensitive to the uncertainties in charge representation discussed in section II. Toward this end we have carried out two sets of simulations of 7-AI in bulk methanol in which the most important charges in the solute and solvent have been systematically varied. The results of such simulations are displayed in Figure 9 and Table 3.

Consider first the effects of varying the charges on the solute "active sites" (top of Figure 9 and Table 3B). Figure 9 shows that the solute−solvent hydrogen-bonding distribution changes markedly with such charge variations. One might intuitively expect that increasing these solute charges and thus its hydrogen bonding to the solvent would lead to enhanced formation of

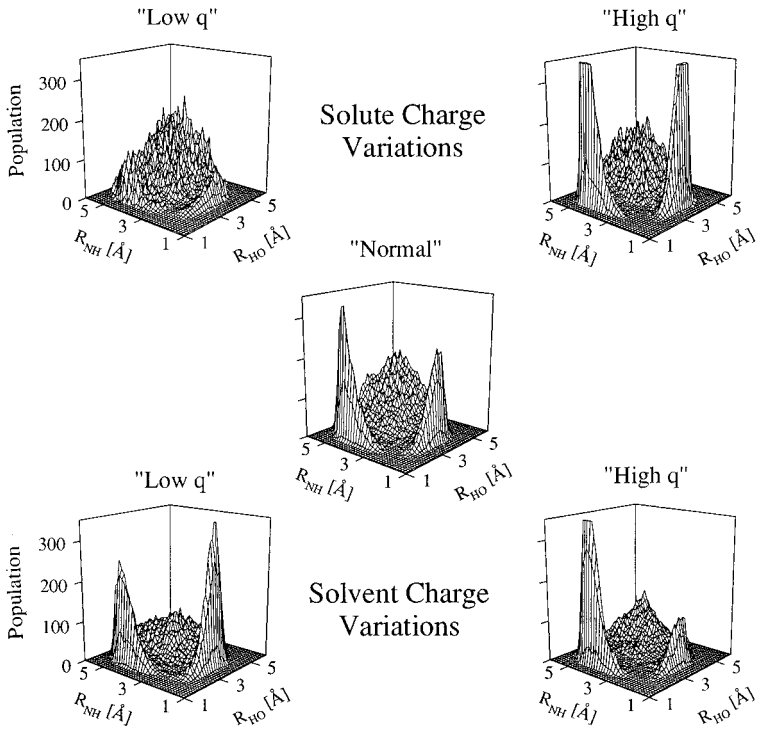

Figure 9. Illustration of the effect of varying the solute and solvent charges on the hydrogen-bonding distance distributions of 7-AI in methanol solution. The meaning of "high" and "low" charge is discussed in the text and defined in Table 3.

cyclic structures. However, just the opposite occurs. The sharpening of the features in Figure 9 with increasing solute charge leads to a reduction in the occurrence of reactive configurations—the values of $f^{\ddagger}$ (Table 3) decrease by factors of between 3 and 6 (depending on $R^{\ddagger}$) for a 0.1*e* increase in charge over the normal values. The reason for this trend is that increasing the strength of the hydrogen bonding between the solute and solvent increases the energy penalty that one must pay to make the poorer hydrogen bonds characteristic of the cyclic structure relative to the hydrogen bonds available in the noncyclic and nonreactive neighbor-bonded structures (Scheme 2).

The variations found when the solvent charges are modified are illustrated in the bottom panel of Figure 9 and listed in Table 3C. As Figure 9 shows, increasing the magnitude of the charge on the solvent O site has the expected effect of increasing the extent of H_U-O_V hydrogen bonding. Although the charge on the solvent H atom is not changed, there is a parallel decrease in the amount of N_U-H_V hydrogen bonding. This change reflects the decreasing availability of solvent H atoms for solute−solvent hydrogen bonding, since they are increasingly tied up in solvent−solvent hydrogen bonds. Table 3C shows that these two opposite trends lead to a net decrease in the fraction of solute molecules cyclically hydrogen-bonded, i.e., to a decrease in the predicted reactivity.

These two sets of simulations provide some calibration of the effects of possible inaccuracies in our potential functions. The semiempirical calculations in Table 1 indicate that electronic excitation of 7-AI or 1-AC probably does not lead to more than a $\pm 0.05e$ change in N_U and H_U atoms involved in hydrogen bonding. The data in Table 3 imply that if the solute charges were incorrect by this amount, the values of $f^{\ddagger}$ calculated would be in error by a factor of ~1.6. In the case of the solvent, this same error in charge would lead to a factor of ~1.4 error in $f^{\ddagger}$. Thus, we conclude that the uncertainties in our predictions of the reactive fractions resulting from uncertainties anticipated in the charge representations used here are comparable to the those incurred by our imprecise knowledge of how to define a reactive geometry. Although these uncertainties warn against placing too much emphasis on small differences in $f^{\ddagger}$ calculated for different alcohols, they do not cloud the basic picture. In particular, it is worth noting that even the largest plausible variations of solute and solvent charge examined here still indicate that only a small fraction (<2% for most definitions of $R^{\ddagger}$) of 7-AI molecules in bulk methanol are in a reactive configuration at any given time. The basic idea of "incorrect" hydrogen bonding being a viable explanation for the slow reaction times observed in bulk alcohols is therefore not in doubt.

D. Solvation Structure and the Solvent Dependence of the Reactive Fractions. We now consider the solvation structures and reactive fractions in a number of different solvents in order to examine whether the differences in simulated values of $f^{\ddagger}$ can account for the variations in reaction rates observed experimentally. As discussed in section II, we have examined two sets of solvent models: the "ab initio" charge model solvents, whose charges were determined from ab initio calculations, and the more standard "OPLS" models of Jorgensen and co-workers.[37−39] We expect the ab initio solvents to be more realistic for the present problem and consider this set to be our primary set. The OPLS models are employed to help assess the sensitivity of the conclusions to choice of solvent representation.

The solvents examined here include the first three normal alcohols methanol through 1-propanol, the fluorinated alcohol 2,2,2-trifluoroethanol ("TFE"), the two nonprimary alcohols 2-proponol and *tert*-butyl alcohol (2,2-dimethyl-2-propanol), and the two dihydroxy solvents ethylene glycol (1,2-ethanediol) and water. Table 4 summarizes the main features of the solvent−solvent hydrogen bonding in the neat solvents. V_{pair} is the interaction energy between a pair of hydrogen-bonded solvent molecules, and R_{pk}, fwhm, and N_C are the positions, widths, and coordination numbers associated with the first peaks in the intermolecular O_V-H_V and O_V-O_V radial distribution functions.

TABLE 4: Solvent−Solvent Hydrogen-Bonding Characteristics

		O−H RDF[b]			O−O RDF[b]		
solvent	$-V_{pair}$[a] (kJ/mol)	R_{pk} (Å)	fwhm (Å)	N_C	R_{pk} (Å)	fwhm (Å)	N_C
methanol	22.5	1.83	0.37	0.97	2.75	0.37	2.02
ethanol	23.4	1.83	0.37	0.95	2.76	0.37	2.01
1-propanol	24.9	1.82	0.36	0.93	2.75	0.35	1.95
2,2,2-trifluoroethanol	19.9	1.95	0.46	0.69	2.82	0.45	1.66
2-propanol	29.7	1.78	0.32	0.97	2.70	0.31	2.00
tert-butyl alcohol	27.9	1.82	0.34	0.93	2.74	0.34	1.94
ethylene glycol	22.9	1.86	0.47	0.82	2.80	0.57	2.54
water	16.0	1.88	0.48	1.80	2.83	0.55	4.50

[a] V_{pair} is the most probable interaction energy between pairs of hydrogen-bonded molecules. [b] R_{pk}, fwhm, and N_C are the position, full width at half-maximum, and number of molecules (coordination number) corresponding to the first peak in the respective radial distribution functions. The coordination number is integrated to the first minimum after R_{pk}.

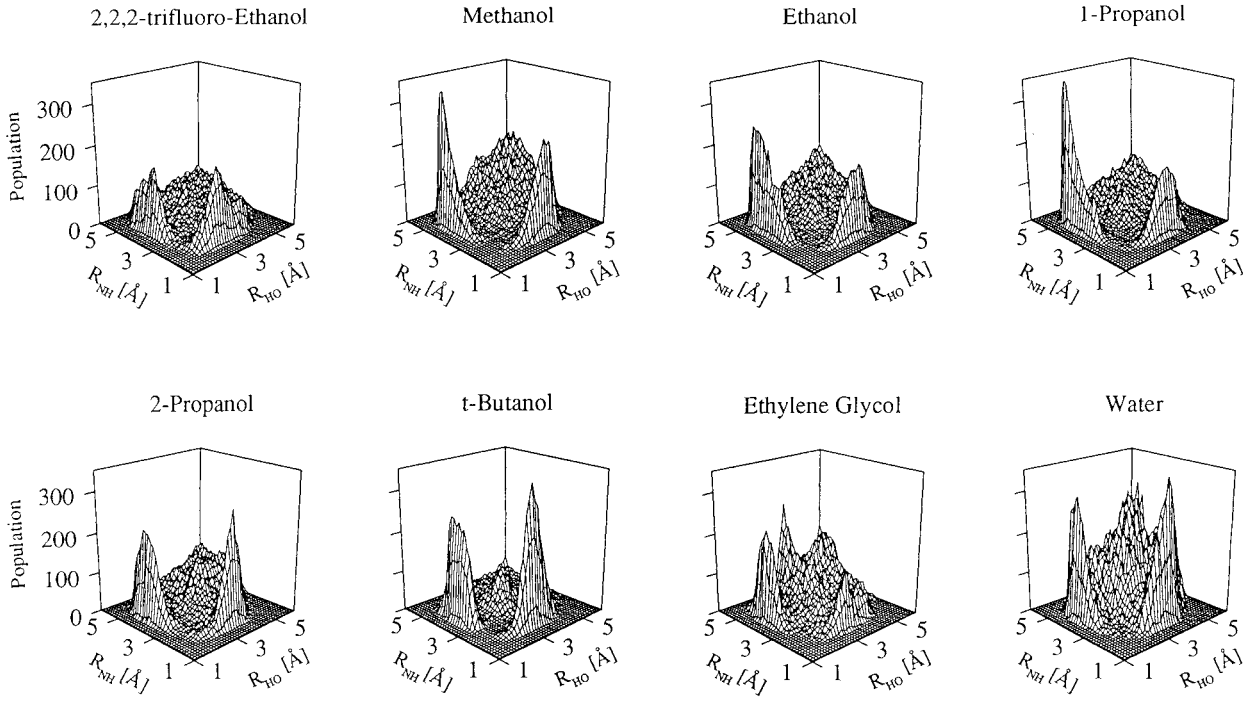

Figure 10. Hydrogen-bonding distance distributions for 7-AI in all of the solvents studied.

From these data one observes that the basic hydrogen-bonding characteristics of all of the monoalcohols, with the exception of TFE, are remarkably similar. The O_V-O_V coordination numbers are all 2.00 ± 0.05, a value that indicates that each solvent molecule acts as a hydrogen bond donor and acceptor virtually 100% of the time. Among this set one finds that the nonprimary alcohols *tert*-butyl alcohol and especially 2-propanol are more strongly hydrogen-bonded (largest V_{pair} and smallest R_{pk} and fwhm values) by virtue of their larger oxygen charges (Table 2). In the case of 2-propanol, this feature is probably exaggerated by the ab initio model compared with the real solvent, on the basis of the fact that the enthalpy of vaporization calculated for this model is too large by 18% (Table 7). 2,2,2-Trifluoroethanol stands out among the monoalcohols as being significantly more weakly hydrogen-bonded, with coordination numbers that reflect the presence of a substantial fraction of broken hydrogen bonds. (This feature may be exaggerated in our TFE model, as discussed in the Appendix.) Finally, ethylene glycol and water differ from the mono-hydroxy solvents in that, especially in water, each solvent molecule is simultaneously hydrogen-bonded to more than two other solvent molecules (i.e., $N_C(O_V-O_V)$ is significantly larger than 2).

We now move to the features of the solvation of 7-AI in these different solvents that should be of importance for determining its reactivity. Relevant data are provided in Figure 10 and Table 5. Figure 10 contains two-dimensional distributions of the R_{NH} and R_{HO} distances of the sort already considered in methanol. The most obvious feature to note from Figure 10 is that all of these solvents exhibit a two-peaked distribution comparable to the bulk methanol case. With the exception of TFE, all of these distributions show very little population (<1%) in structures that we deem reactive. But before discussing the calculated fractions, we first consider in more detail how the solute−solvent bonding structure varies with solvent. We do so using the results in Table 5, which summarizes characteristics of the distributions of N_U-H_V and H_U-O_V distances observed. In the first two columns under each of these headings some features of the one-dimensional radial distribution functions of these two H-bonding distances are listed. The interaction energies ("V_{UV}") are pair energies between the solute and the particular solvent molecule that is closest to the solute site of interest. These values are indicative of the strength of the hydrogen bonds made to each of the solute active sites. The next four columns characterize the average positions ($\langle R \rangle$) and widths (standard deviations, δR) of the peaks observed in the two-dimensional distributions depicted in Figure 10.

The data in Table 5 indicate that the solute−solvent bonding is fairly similar in most of these solvents. It is also comparable

TABLE 5: Structural Characteristics of Solvation in Various Solvents[a]

	N_U-H_V Bonding[b]							H_U-O_V Bonding[b]								
	1D rdfs			2D distributions				1D rdfs			2D distributions				Structure[c]	
solvent[a]	R_{pk} (Å)	N_C	$-V_{UV}$ kJ/mol	$\langle R_1\rangle$ (Å)	δR_1 (Å)	$\langle R_2\rangle$ (Å)	δR_2 (Å)	R_{pk} (Å)	N_C	$-V_{UV}$ kJ/mol	$\langle R_1\rangle$ (Å)	δR_1 (Å)	$\langle R_2\rangle$ (Å)	δR_2 (Å)	%8	%nn
7-Azaindole																
methanol	1.93	0.88	26.2	2.06	0.21	3.80	0.51	1.83	1.00	24.9	1.98	0.23	4.57	0.57	7	91
ethanol	1.94	0.71	24.9	2.03	0.21	3.82	0.47	1.81	1.00	29.4	1.90	0.20	4.22	0.64	16	79
1-propanol	1.95	0.75	28.4	2.09	0.21	3.76	0.54	1.81	0.98	30.0	1.92	0.20	4.49	0.59	18	71
TFE	2.04	1.09	19.0	2.16	0.21	3.44	0.71	1.89	0.91	33.2	2.08	0.25	4.06	0.94	22	64
2-propanol	1.89	0.90	30.4	2.05	0.21	3.62	0.49	1.81	0.89	26.9	1.97	0.27	4.23	0.69	3	92
tert-butyl alcohol	1.91	1.08	36.4	2.02	0.19	3.48	0.51	1.80	0.95	27.5	1.92	0.21	3.86	0.61	32	51
ethylene glycol	1.98	0.66	19.4	2.13	0.22	3.66	0.66	1.81	1.24	23.4	1.97	0.24	4.17	0.63	14	72
water	1.96	1.28	18.1	2.15	0.23	3.84	0.54	1.83	0.99	23.4	2.02	0.25	4.19	0.56	1	98
1-Azacarbazole																
methanol	1.91	0.98	27.1	2.07	0.21	3.98	0.52	1.82	1.03	27.4	1.93	0.20	4.48	0.61	9	88
water	1.97	1.08	18.7	2.15	0.23	3.75	0.54	1.80	1.02	24.3	1.98	0.24	4.20	0.56	3	97

[a] TFE denotes 2,2,2-trifluoroethanol. [b] R_{pk} and N_c are the peak position and coordination number associated with the first peak in the one-dimensional radial distribution functions ("rdfs") of the two solute−solvent H-bonding coordinates N_U-H_V and H_U-O_V. Coordination numbers were determined from the integral under this first peak out to the first minimum in the rdf (~2.75 Å in R_{NH} and ~2.65 Å in R_{HO}). V_{UV} is the most probable interaction energy between the solute and the solvent molecule hydrogen-bonded to the particular site (i.e. the particular solvent molecule with the shortest R_1 distance). The four columns under the heading "2D distributions" characterize the average positions ($\langle R\rangle$) and widths (standard deviations, δR) of the peaks observed in the two-dimensional distributions depicted in Figure 10. The superscripts "1" and "2" label values in primary and secondary dimensions of these plots. For example, in the column $\langle R_1\rangle$ under the heading N_U-H_V are the average R_{NH} distances found for the peaks on the right side of the distributions in Figure 10. These are primarily representative of N_U-H_V hydrogen bonding. The values of δR_2 under this same heading are the widths of this peak in the other, i.e., the R_{HO} dimension. These values provide some indication of the "tightness" of the hydrogen bonding between the solute and solvent at the solute active sites. [c] "%8" and "%nn" refer to the relative frequency of the noncyclic configurations sampled that are hydrogen-bonded in a manner characteristic of "eight-membered" and "nearest-neighbor bonded" structures, as schematically shown in Scheme 2.

to the hydrogen bonding that takes place within the solvents themselves. The coordination numbers show that in nearly all cases the N_U and H_U solute sites form hydrogen bonds to (distinct) solvent molecules more than 75% and 95% of the time, respectively. Some differences among the various solvents can also be discerned. For example, although the energies at the two solute sites are usually comparable (and close to V_{pair}), hydrogen bonds to the N_U site can be either stronger or weaker than those at the H_U site. In TFE the difference is most marked. Here, the bonding to the N_U site is relatively weak, as are hydrogen bonds in the neat liquid, whereas the H_U site bonding is uncommonly strong, owing to the reduced charge on the hydroxyl oxygen atom (Table 2).[54] A final aspect of the solvation structure that shows significant variations among the different solvents involves the relative disposition of the two solvent molecules that are hydrogen-bonded to the solute. This aspect is represented in the last two columns of Table 5, where we list the frequency of occurrence of the eight-membered ring ("%8") and nearest-neighbor ("%nn") structures defined in Scheme 2. The preference for forming eight-membered ring structures versus neighbor-bonded structures generally decreases as the density of available OH bonds in the solvent increases. Thus, the %8 values increase in the order water < methanol < ethanol < 1-propanol < *tert*-butyl alcohol. A notable exception in this series is 2-propanol, which forms fewer eight-membered rings than would be expected on this basis. In this solvent (and not others) solvent−solvent bonds are stronger than solvent−solute hydrogen bonds so that nearest-neighbor bonding is strongly preferred for energetic reasons.

Having characterized the basic structural features of the active-site hydrogen bonding, we now turn to the reactive fractions $f^{\ddagger}$ determined in the different solvents. These results are summarized in Table 6 and Figure 11. In Table 6 we list reactive fractions for the definitions of reactive geometry discussed previously: $R^{\ddagger} = 2.19$, 2.44, and 2.69 Å. Also listed for the $R^{\ddagger} = 2.19$ Å case are the values of τ_{PT} and $\Delta G^{\ddagger}$ they imply. (Recall that we expect that the smallest value of $R^{\ddagger}$ should represent the most realistic choice.) Consistent with the distributions displayed in Figure 10, the reactive fractions calculated using this most restrictive definition are all quite small—less than 2% in all cases. In the normal alcohol series there is a systematic decrease in the reactive fraction (for all $R^{\ddagger}$) in the order methanol > ethanol > 1-propanol. This trend parallels the experimentally observed trend in reaction rates.[12,13] TFE has by far the largest population of reactive species, $f^{\ddagger} \approx$ 1.6%, which is consistent with the experimental observation of very rapid reaction in this solvent.[13] Alternatively, the reactive fractions determined in ethylene glycol and water are smaller than those in the normal alcohols, which is again consistent with the slower reaction observed in these two solvents.[13,14]

In addition to these qualitative trends, the reactive fractions calculated for 7-AI in these six solvents are in semiquantitative agreement with the idea that the rates are simply proportional to $f^{\ddagger}$. This point is illustrated in Figure 11 where the observed reaction rates are plotted as a function of $f(R^{\ddagger} = 2.19$ Å). With the exception of water, all of the data in these six solvents can be fit to eq 1.1 using a value of $k_{PT} = 3.3$ ps^{-1} (or $\tau_{PT} = 300$ fs). In light of what is known about the 7-AI reaction in isolated catalytic complexes, such a rate constant seems quite reasonable.[4] In the case of water, the calculated fraction is roughly 2-fold larger than expected on the basis of this correlation. If the reactive fractions are assumed correct, these results would imply a roughly 2-fold slower proton transfer ($\tau_{PT} \approx 0.6$ ps) in water[55] compared with that in the primary alcohols. Isotope effect data[15,21] indicate that there may in fact be some quantitative differences in the proton-transfer step (k_{PT}) in water compared with that in alcohol solvents, so this computed difference in reactive fractions could in fact be correct. However, given the variations in $f^{\ddagger}$ provided by different water models, it is unwise to attach much significance to the deviation. With respect to all of the aforementioned solvents, including water, it is best to conclude that the simulation results are

TABLE 6: Summary of Reactive Fractions[a]

solvent	$R^{\ddagger} = 2.19$ Å $f(R^{\ddagger})$ (10^{-3})	τ_{PT} (ps)	$\Delta G^{\ddagger}$ (kJ/mol)	$R^{\ddagger} = 2.44$ Å $f(R^{\ddagger})$ (10^{-3})	$R^{\ddagger} = 2.69$ Å $f(R^{\ddagger})$ (10^{-3})
7-Azaindole−Ab Initio Solvent Models					
methanol	2.5 ± 0.4	0.3	15.0	9.0 ± 1.3	20 ± 2
ethanol	1.3 ± 0.2	0.2	16.6	4.7 ± 0.5	13.5 ± 1.7
1-propanol	1.2 ± 0.4	0.2	16.8	4.3 ± 1.0	12.5 ± 1.2
TFE	16 ± 2	0.5	10.3	68 ± 7	146 ± 11
2-propanol	5 ± 3	2	13	16 ± 8	31 ± 12
tert-butyl alcohol	7 ± 3	2	12	19 ± 5	48 ± 4
ethylene glycol	0.8 ± 0.4	0.3	18	12 ± 4	41 ± 11
water	0.66 ± 0.08	0.5	18.3	5.2 ± 0.4	19.4 ± 0.9
7-Azaindole−Other Solvent Models					
methanol (opls)	2.3 ± 0.5	0.3	15.0	7.1 ± 1.1	15 ± 1.2
ethanol (OPLS)	1.5 ± 0.4	0.2	16.1	7.5 ± 1.1	24 ± 2
1-propanol (OPLS)	0.8 ± 0.2	0.2	17.6	3.2 ± 0.6	10 ± 2
2-propanol (OPLS)	2.6 ± 1.2	0.6	15	5.5 ± 1.5	18 ± 7
tert-butyl alcohol (OPLS)	4 ± 2	1.3	14	17 ± 2	65 ± 13
water (SPC)	1.0 ± 0.3	0.8	17	5.5 ± 1.2	23 ± 3
water (TIP4P)	2.0 ± 1.0	1.6	15	8 ± 4	30 ± 11
1-Azacarbazole−Ab Initio Solvent Models					
methanol	2.3 ± 0.7	1.2	15	8 ± 2	18 ± 4
water	0.8 ± 0.3	2	18	5 ± 2	23 ± 4

[a] Reactive fractions $f(R^{\ddagger})$ are the fractional populations contained within regions ($R_{NH} \leq R^{\ddagger}$, $R_{HO} \leq R^{\ddagger}$), where R_{NH} and R_{HO} are the solute−solvent hydrogen-bonding distances defined in Figure 3. τ_{PT} is the proton-transfer rate that would be required for a given $f(R^{\ddagger})$ in order to obtain the experimentally observed reaction rate (k_{obs} values from refs 13 and 21) according to eq 1.1. Uncertainties in the values of $f(R^{\ddagger})$ listed here are ±1 standard deviation of the mean of 10 subsets of the overall simulation

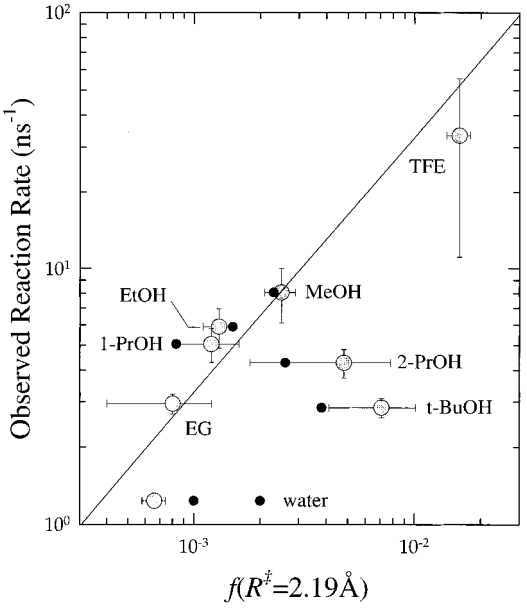

Figure 11. Comparison of simulated reactive fractions and observed reaction rates of 7-AI in bulk alcohol solvents. The larger symbols are results obtained using the ab initio solvent set, and the smaller symbols are those obtained with OPLS models. The line shown is the best fit of the ab initio data (in a linear format) excluding 2-propanol and *tert*-butyl alcohol. It represents the proportionality $k_{obs} = (3.3\ ps^{-1})\ f^{\ddagger}$.

consistent with the main solvent dependence of these reactions deriving from the equilibrium fractions $f^{\ddagger}$, as proposed on the basis of experimental results.[21]

However, Figure 11 also clearly shows that two of the solvents studied here, the two nonprimary alcohols 2-propanol and *tert*-butyl alcohol, do not fit neatly into this picture. The reactive fractions in these two solvents are significantly larger than the fractions in methanol, whereas the observed reaction rates are actually much smaller. There is about a factor of 5 discrepancy between the calculated fractions and what would be expected based on the results in the other solvents. This "deviant" behavior can be interpreted in a number of ways. One interpretation would be to conclude that the focus on $f^{\ddagger}$ alone is incorrect. Differences in k_{PT} between primary and secondary/tertiary alcohols could just as well give rise to the different reaction rates in these systems. Or, contrary to the test cases studied in section III.B, the *dynamics* of solvation could be important in these particular solvents. Although these possibilities cannot be ruled out entirely, given the extensive experimental data implicating an equilibrium solvent property like $f^{\ddagger}$ as being the sole solvent effect,[21] it seems unlikely that this underlying idea is incorrect. A more likely interpretation is that the equilibrium fractions of these solvents are not accurately portrayed by the present simulations, probably as a result of inaccuracies in the intermolecular potential functions used for these solvents. Some perspective on this possibility can be gleaned from the results on OPLS solvents also provided in Table 6 and Figure 11. We note that the different charges in the OPLS and ab initio models produce roughly 2-fold differences in the values of $f^{\ddagger}$ predicted in the case of 2-propanol and *tert*-butyl alcohol but much smaller differences in the case of the normal alcohols. These differences reflect only the choice of charge representation. It may also be that our use of united-atom representations of CH_2 and CH_3 groups does not do justice to the steric interactions in these solvents, which would be expected to be significantly different from those in primary alcohols. A final possibility is that both the basic idea and the simulation models are basically sound but that our use of the criterion $R_{NH} = R_{HO} = 2.19$ Å to define reactive configurations is too crude. We note that there are some differences between the distributions of H-bonding angles in the cyclic forms of primary and these secondary/tertiary alcohols that perhaps are important. Recent high-resolution jet studies indicate that 7-AI−H_2O complexes may be cyclic in the sense defined here but nevertheless nonreactive owing to angular displacements that are difficult to overcome at the low temperatures achieved in supersonic expansion.[56] However, until more is known about the real geometric constraints involved, it does not seem fruitful to try to adopt more complicated criteria in order to better correlate all of the solvents.

With these considerations in mind, we conclude that the results presented in Table 5 and Figure 11 generally support the notion that the variation in the reaction rates of 7-AI in bulk alcohols and water is due mainly to variations the equilibrium populations of reactive forms, as described by eq 1.1. Indeed, given the simplicity of the modeling performed here, the fact that all of the experimental results can be rationalized using the simulated fractions and values of k_{PT} (or τ_{PT} in Table 5) that are all near the expected value of ~0.5 ps should probably be viewed as strong support for the basic picture discussed in the Introduction.

It is therefore interesting to consider what differences in solvation are responsible for the different reactive fractions and thus reaction rates in these various solvents. We have not discerned any clear links between the relatively subtle variations in solvent structure observed in the different alcohol solvents and differences in their reactive fractions. However, there is a clear connection between $f^{\ddagger}$ and the energetics of solvation. At least in the mono-hydroxy alcohols, the origin of the solvent dependence of $f^{\ddagger}$, or equivalently of $\Delta G^{\ddagger}$, can be simply explained on the basis of the pair bonding energies of the reactive and nonreactive forms. Assuming that every alcohol molecule has strong interactions with exactly two other alcohol molecules (invalid in the cases of water and ethylene glycol), an accounting of the energy cost of adopting a reactive geometry in a bulk alcohol solvent can be made according to the approximate relation

$$\Delta E_{cyc} \cong \{V(\text{cyc}) + 2V(vv)\} - \{V(\text{U}, 1) + V(\text{U}, 2) + V(1, 3) + V(2, 4)\} \quad (3.6)$$

In this expression we consider the energetics of the two key solvent molecules labeled "1" and "2" in Scheme 2, which we assume make a total of four hydrogen bonds to other molecules. The $V(x)$ are average interaction energies of various solute−solvent and solvent−solvent pairs x, averaged over distributions of the sort illustrated in Figure 4. The energy of a nonreactive neighbor-bonded or eight-membered ring structure is given by the second term in braces in eq 3.6. $V(U, 1)$ in this latter term refers to the interaction energy between the solute ("U") and solvent molecule 1, defined as the particular solvent molecule having the minimum N_U-H_V distance, and $V(1, 3)$ is the interaction energy between this solvent molecule and whichever other solvent molecule ("3") has the smallest O_V-H_V distance. $V(\text{U}, 2)$ and $V(2, 4)$ are defined analogously. (In eight-membered ring structures, labels "3" and "4" refer to the same solvent molecule whose interactions are included twice in the accounting procedure.) The energy of the cyclic structure is estimated as the average interaction energy simulated for an isolated 1:1 complex in cyclohexane, $V(\text{cyc})$, plus the energy of two solvent−solvent bonds that solvent 2 makes once freed from the solute. The latter energy is from the average bulk pair energy $V(vv)$.

A comparison of these cyclic energy estimates ΔE_{cyc} with the actual free energies $\Delta G^{\ddagger}$ is provided in Figure 12. Although the above accounting scheme only considers four pair interactions, the values of ΔE_{cyc} are nearly within uncertainties of the values of $\Delta G^{\ddagger}$ in the mono-alcohol solvents. The only exception is *tert*-butyl alcohol, for which ΔE_{cyc} is nearly 10 kJ/mol greater than $\Delta G^{\ddagger}$. From this remarkable agreement we conclude that in all but one of these solvents, the primary determinant of the reactive fraction is simply the differential strength of the hydrogen bonds that can be formed in cyclic versus noncyclic structures. With the exception of *tert*-butyl alcohol, entropic considerations must therefore play a minor role in determining

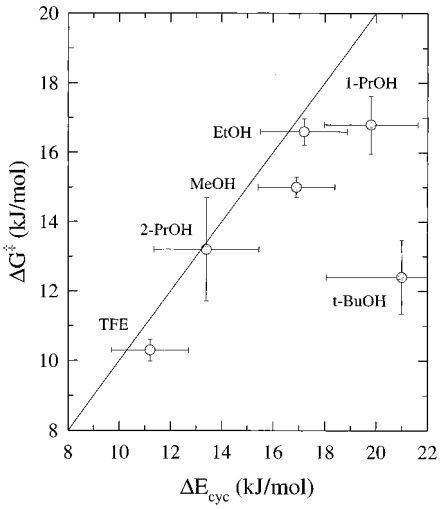

Figure 12. Comparison of the approximate energy (ΔE_{cyc}, eq 3.6) with the free energy ($\Delta G^{\ddagger}$, eq 1.1) required to form cyclic structures. The line represents equality between these two energies.

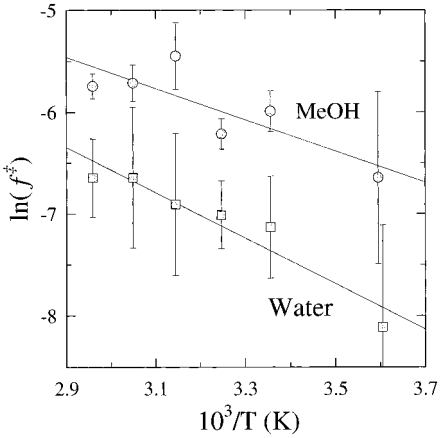

Figure 13. Arrhenius plots of the temperature dependence of the reactive fractions of 7-AI in methanol and water.

$f^{\ddagger}$ in these mono-alcohols. (Water is also an exception, as is discussed in the next section.)

E. Temperature and Solute Dependence. Two final aspects of the simulated behavior lend further support to the notion that the reactive fractions are primarily responsible for the solvent dependence of the reaction rates in these systems. The first involves the temperature dependence of $f^{\ddagger}$. Experimentally, the rates of the 7-AI and 1-AC reactions are observed to exhibit activation energies of ~10−15 kJ/mol in a variety of alcohol solvents.[21] Within the context of eq 1.1, this activation energy for reaction is interpreted as being the enthalpy change in forming the reactive form.[57] As a further test of the model, we have therefore performed simulations of 7-AI in methanol and water for six temperatures in the range 275−340 K. The results are displayed as Arrhenius plots in Figure 13. These plots yield values of $\Delta H^{\ddagger}$ of 13 ± 4 and 11 ± 3 kJ/mol for methanol and water, respectively. The activation energies observed experimentally for the 7-AI reaction are 10.4 ± 0.4 kJ/mol[58] in methanol and 8.8 ± 1 kJ/mol[14] in water. Thus, the observed activation energies for reaction in both solvents are within uncertainties of the temperature dependence of the simulated reactive fractions ($\Delta H^{\ddagger}$), supporting the above interpretation.

It is interesting to compare these values of $\Delta H^{\ddagger}$ with the results calculated in part D. In the case of methanol the simulated value of $\Delta H^{\ddagger}$ is consistent with both the estimate of

ΔE_{cyc} derived previously (17 ± 2 kJ/mol) and $\Delta G^{\ddagger}$ itself (15.0 ± 0.3 kJ/mol), as anticipated. In water, on the other hand, the activation energy appears to be significantly lower than the value of $\Delta G^{\ddagger} = 18.3 \pm 0.3$ kJ/mol. (Estimates of ΔE_{cyc} also lead to values significantly lower than $\Delta G^{\ddagger}$.) These differences could reflect the fact that entropic as well as energetic effects play a role in determining $f^{\ddagger}$ in water. The entropic contribution appears to be large in this case, accounting for more than a 10-fold reduction in $f^{\ddagger}$ compared with what would be expected on energetic grounds alone. Since this conclusion rests on the accuracy of our $\Delta G^{\ddagger}$ estimates, which are by no means assured, it is comforting to note that there is also experimental evidence for such a distinction between water and most alcohol solvents. By use of the notation of eq 1.1, the ratio $k_{obs}/\exp(-E_a/(RT))$, where E_a is the experimentally observed activation energy, should be approximately constant if $\Delta G^{\ddagger} \cong E_a$.. For the 7-AI and 1-AC reactions in alcohols this ratio appears to be approximately constant among the normal alcohols but roughly an order of magnitude larger in water,[21] in complete agreement with the simulation results.

The final aspect of these reactions we consider is their solute dependence. As discussed in the Introduction, striking parallels between the solvent dependence of the tautomerization rates of 7-AI and 1-AC have been observed experimentally.[20,21] This observation has been interpreted within the context of eq 1.1 as reflecting the fact that the solvent dependence of $f^{\ddagger}$ is nearly the same for these two solutes. Given the similarity in their active-site geometries and charges (Table 1), such closeness is not surprising. Nevertheless, it is important that the simulations bear out this expectation. As displayed in Table 5, the simulated features of the solute−solvent hydrogen bonding differ little between 7-AI and 1-AC. The slightly larger charges on the active sites of 1-AC lead to a small enhancement of the hydrogen bonding to both sites relative to 7-AI, as indicated by the decrease in R_{pk} and the increase in N_C and V_{UV}. However, these modest changes do not significantly alter the reactive fractions calculated, as indicated by the comparison provided in Table 6. Thus, with respect to both the solute and temperature dependence of the reactive fractions, the present simulations appear to corroborate the picture of the solvent involvement constructed to explain the experimental data.

IV. Summary and Conclusions

In this work we have used classical Monte Carlo and molecular dynamics computer simulations to explore the role played by hydroxylic solvents in the excited-state tautomerization of 7-azaindole and 1-azacarbazole. We have examined the solvation structure in a variety of 7-AI− and 1-AC−alcohol and water systems with a view toward testing the mechanism of solvent catalysis proposed on the basis of experimental work.[21] This mechanism postulates that the slow tautomerization observed in bulk alcohol solvents results from the scarcity of reactant molecules properly solvated for reaction. "Proper" solvation is assumed to involve a cyclically hydrogen-bonded complex with a single alcohol solvent molecule bridging the sites of proton transfer. The mechanism further supposes (eq 1.1) that the rates observed in different bulk solvents are proportional to the equilibrium fraction of molecules in the reactive geometry, with the proportionality constant being the rate of the actual proton-transfer step (k_{PT}), which is assumed to be rapid (<5 ps) and solvent-independent.

The simulations performed here generally support this proposed mechanism. In all of the bulk solvents examined, which included six alkyl alcohols, ethylene glycol, and water, the fraction of solute molecules in "reactive" solvation states ($f^{\ddagger}$) was observed to be small, typically less than 1%. Molecular dynamics simulations in methanol and water showed these reactive fractions, and not solvent dynamical effects, should control the reaction rates, as is assumed in eq 1.1. In most of the solvents studied a good correlation was found between the simulated reactive fractions and the rates experimentally measured for the 7-AI reaction (Figure 11). This correlation implies a value of $k_{PT} \approx (0.3\ \text{ps})^{-1}$ for the rate of the proton-transfer step in properly solvated 7-AI−alcohol complexes, a value consistent with what is known about reaction rates in dilute solution. Most of the results reported here involved simulations of the 7-AI reaction. However, several simulations of the 1-AC solute indicate that the reactive fractions in the 1-AC system should be very close to those in 7-AI. This finding is consistent with the remarkable parallelism observed in the solvent dependence of the two reactions. Finally, we also simulated the temperature dependence of the reactive fractions of 7-AI in two solvents: methanol and water. The agreement between the enthalpy changes associated with formation of reactive solvation states and the activation energies observed experimentally in these two solvents lends further support to the validity of the proposed mechanism.

Two of the eight solvents studied here, the two nonprimary alcohols 2-propanol and *tert*-butyl alcohol, were observed to deviate significantly from the correlation established by the other solvents. The values of the reactive fractions calculated in these two solvents are roughly 5-fold larger than expected on the basis of the experimentally observed reaction rates. Of the possible reasons considered for these deviations, it seems most likely that inaccuracies in the intermolecular potential models used here are primarily to blame. Some tests of the sensitivity of the simulated behavior to variations in the potential parameters were performed in the present work, and from these it can be concluded that an accuracy of no better than a factor of 2 should be expected for the values of the reactive fractions calculated here. Although relative variations among similar solvents should be better reproduced, it seems reasonable to suspect that possibly subtle differences between solvation in primary and secondary alcohols might not be captured by the simple potential functions employed. We are currently performing simulations of the solvatochromic behavior of solutes sensitive to hydrogen bonding in order to explore just what level of realism is to be expected from different potential models of alcohol solvents.[59]

Despite these difficulties, the present simulations provide considerable evidence that the mechanism of solvent involvement inferred from experimental evidence is basically correct. What further insight do the simulations offer regarding the nature of solvation/reaction in these systems? One observation is that in most respects solvation of 7-AI and 1-AC is not qualitatively different in water compared with solvation in alcohol solvents. Dynamical studies show that reorganization of the solvation structure in water occurs on a 10−100 ps time scale, making the idea that long-lived solvation states block reaction in water for times in the nanosecond range appear untenable. In water and in alcohol solvents, the *dynamics* of solvation appear to be irrelevant to the reaction. The slower reaction times observed in water compared with those in alcohol solvents merely reflect the smaller fraction of reactive (cyclically bonded) forms present. The reason for the small proportion of reactive solvation states in water and in hydroxylic solvents in general is geometrical in nature. The hydrogen-bonding sites in 7-AI and 1-AC are positioned such that a single water or alcohol molecule simultaneously bound to both sites can only make

TABLE 7: Thermodynamic Properties of the Neat Solvents[a]

	density (g cm^{-3})			ΔH_{vap} (kJ/mol)[b]		
solvent	expt	ab initio	OPLS	expt	ab initio	OPLS
methanol	0.786	0.758(−4)	0.759(−3)	37.4	35.8(−4)	37.9(+1)
ethanol	0.785	0.811(+3)	0.748(−5)	42.3	42.7(+1)	41.8(−1)
1-propanol	0.800	0.835(+4)	0.788(−1)	47.3	46.2(−2)	47.4(+0)
TFE	1.374	1.088(−21)		43.4	38.7(−11)	
2-propanol	0.781	0.772(−1)	0.779(−0)	45.5	53.8(+18)	47.0(+3)
tert-butyl alcohol	0.781	0.755(−3)	0.773(−1)	46.8	46.1(−2)	46.4(−1)
ethylene glycol	1.110	1.075(−3)		67.8	78.7(+16)	
water[c]	0.997	0.912(−9)	0.999(+0)	44.0	36.9(−16)	44.6(+1)

[a] All values correspond to 298 K and 1 atm pressure. Values in parentheses are the percentage errors in the simulated values. OPLS and experimental values taken from the compilations in refs 38 and 39. [b] Enthalpies of vaporization were calculated from the total interaction energies observed in the simulation using an experimental correction for gas nonideality as discussed in ref 38. [c] The OPLS values listed for water are for the preferred TIP4P model.[39]

relatively weak, highly nonlinear hydrogen bonds to the solute (Figure 5). In bulk solvents, eight-membered ring or neighbor-bonded structures (Scheme 2) prevail over cyclically bonded forms simply because stronger hydrogen bonds can be formed when two different solvent molecules bind to the solute "active sites". In most of the solvents studied here the free energy change to reach the reactive geometry can be accurately accounted for simply in terms of the energy penalty associated with exchanging two strong hydrogen bonds made in the nonreactive structures for the two weaker bonds made in the cyclic form. Entropic effects are therefore of little importance in the reactive equilibrium in most alcohol solvents. It is interesting to note that water is qualitatively different in this regard. In water, the reactive fraction is significantly smaller than is accounted for by this energy effect alone such that there must also be a sizable entropy penalty to adopting the reactive geometry in water.

We can summarize the findings of the present work by stating that the reaction rates of 7-AI and 1-AC in hydroxylic solvents can be understood in terms of geometric hydrogen-bonding requirements between the solute and solvent molecules. Such geometric control over the reaction is of course rather specific to these particular solutes and solvents, as discussed in section IIIA (Figures 5 and 6.). It is therefore of interest to examine these same reactions in other solvent types (such as amides[60]) as well as other reactions, for example, DPC[46] (Figure 6) and 7-hydroxyquinoline,[42] in alcohol solvents in order to form a more complete picture of the role of solvation structure and dynamics in solvent-catalyzed proton-transfer processes. Work along these lines is currently in progress in our group.

Acknowledgment. The authors acknowledge the generosity of Bill Jorgensen in providing a copy of the "BOSS" program for performing Monte Carlo simulations of general solute−solvent systems. Without the use of this program many of the simulations reported here would not have been possible. We also thank Tami Marrone for performing some of the initial simulations on these systems. Some of this work was partially supported by funds from the National Science Foundation and from the Office of Naval Research.

Appendix

To check the reasonableness of the "ab initio" potential models used here, we have compared the solvent−solvent radial distribution functions, densities, and enthalpies of vaporization of the pure liquids with results obtained with the OPLS models[38,39] and from experiment. Some characteristics of the radial distribution functions and pair interaction energies of the ab initio models are provided in Table 4 of the main text. From comparisons to OPLS results (available for all solvents except for TFE and ethylene glycol) for these and other structural/energetic properties, the neat solvents showed the ab initio models to be quite similar to the OPLS models in almost all cases. Table 7 summarizes the comparison of the densities and enthalpies of vaporization (ΔH_{vap}) obtained with the ab initio and OPLS models with the experimental values. These data show that in cases of overlap, the ab initio properties deviate more from the experimental values than their OPLS counterparts. The average absolute error in the simulated densities is 4% for the ab initio parametrization and 2.5% for the OPLS parametrization. In the case of ΔH_{vap} the errors are 7% (ab initio) versus 1.5% (OPLS). The better agreement for the OPLS set is to be expected, since the parameters of these models were optimized in order to reproduce these specific experimental quantities. (For consistency with the other representations we have used a three-site model for water, whereas the properties reported here are for the preferred four-site (TIP4P[39]) version.) Nevertheless, in nearly all cases the agreement between the calculated and experimental values appears to be acceptable. The ab initio models of 2-propanol and ethylene glycol are too strongly bound by some 15−20% whereas water is too weakly bound by 16%. These departures from experimental results should probably be expected to give rise to some quantitative inaccuracies in the results obtained here but to still be qualitatively reliable. However, this may not be true in one solvent, TFE. There is no OPLS model of this solvent. We have therefore adopted Lennard-Jones parameters for the CF_3 group from another source.[40] These parameters, combined with our ab initio charges lead to a system with a much lower density (>20% lower!) than is observed experimentally. ΔH_{vap} is also smaller than the experimental value by some 11%. Given the large deviation in density, it seems prudent to view the results obtained with this solvent model with some caution. We are currently looking for a better potential model with which to represent this particular solvent.

Supporting Information Available: Table listing solute coordinates and parameters (1 page). Ordering information is given on any current masthead page.

References and Notes

(1) Ingham, K. C.; El-Bayoumi, M. A. *J. Am. Chem. Soc.* **1974**, *96*, 1674.

(2) Share, P.; Pereira, M.; Sarisky, M.; Repinec, S.; Hochstrasser, R. M. *J. Lumin.* **1991**, *48*−*49*, 204.

(3) Takeuchi, S.; Tahara, T. *Chem. Phys. Lett.* **1997**, *277*, 340.

(4) Reynolds, L. E.; Maroncelli, M. Manuscript in preparation.

(5) Douhal, A.; Kim, S. K.; Zewail, A. H. *Nature* **1995**, *378*, 260.

(6) Fuke, K.; Tsukamoto, K.; Misaizu, F.; Kaya, K. *J. Chem. Phys.* **1991**, *95*, 4074.
(7) Chang, C.-P.; Hwang, W.-C.; Meng-Shin, K.; Chou, P.-T.; Clements, J. H. *J. Phys. Chem.* **1994**, *98*, 8801.
(8) Chou, P.-T.; Wei, C.-Y.; Chang, C.-P.; Chiu, C.-H. *J. Am. Chem. Soc.* **1995**, *117*, 7257.
(9) Avouris, P.; Yang, L. L.; El-Bayoumi, M. A. *Photochem. Photobiol.* **1976**, *24*, 211.
(10) Herbich, J.; Sepiol, J.; Waluk, J. *J. Mol. Spectrosc.* **1984**, *114*, 329.
(11) McMorrow, D.; Aartsma, T. J. *Chem. Phys. Lett.* **1986**, *125*, 581.
(12) Konijnenberg, J.; Huizer, A. H.; Varma, C. A. G. O. *J. Chem. Soc., Faraday Trans. 2* **1988**, *84*, 1163.
(13) Moog, R. S.; Maroncelli, M. *J. Phys. Chem.* **1991**, *95*, 10359.
(14) Chapman, C. F.; Maroncelli, M. *J. Phys. Chem.* **1992**, *96*, 8430.
(15) Smirnov, A. V.; English, D. S.; Rich, R. L.; Lane, J.; Teyton, L.; Schwabacher, A. W.; Luo, S.; Thornburg, R. W.; Petrich, J. W. *J. Phys. Chem. B* **1997**, *101*, 2758. Chen, Y.; Rich, R. L.; Gai, F.; Petrich, J. W. *J. Chem. Phys.* **1993**, *97*, 1770, 2106. Gai F.; Chen Y.; Petrich, J. W. *J. Am. Chem. Soc.* **1992,** *114*, 8343.
(16) Chen, Y.; Gai, F.; Petrich, J. *Chem. Phys. Lett.* **1994**, *222*, 329.
(17) Chen, Y.; Gai, F.; Petrich, J. W. *J. Am. Chem. Soc.* **1993**, *115*, 10158.
(18) Chou, P.-T.; Martinez, M. L.; Cooper, W. C.; McMorrow, D.; Collins, S. T.; Kasha, M. *J. Phys. Chem.* **1992**, *96*, 5203.
(19) Waluk, J.; Kamorowski, S. J.; Herbich, J. *J. Phys. Chem.* **1986**, *90*, 3868.
(20) Boryschuck, S. J. The Excited-State Double Proton Transfer Reaction of 1-Azacarbazole in Alcohols. MS Thesis, Penn State University, University Park, PA, 1993. See also the following. Chapman, C. F. Time-Resolved Fluorescence Studies of Solvation Dynamics and Chemical Reaction. Ph.D. Thesis, Penn State University, University Park, PA, 1992.
(21) Reynolds, L. E.; Boryschuk, S. J.; Chapman, C. F.; Maroncelli, M. The Excited-State Tautomerization of 1-Azacarbazole and 7-Azaindole in Hydroxylic Solvents: A Revised View of the Solvent's Role. Manuscript in preparation.
(22) In ref 16 Petrich and co-workers suggested that the differences in reaction rates of 7-AI in different alcohols may be due to differences in the acidity of different alcohols affecting the actual proton-transfer step. In our view, the fact that the isotope effect does not vary substantially over a range of alcohol solvents makes this interpretation seem unlikely.
(23) Note that our notation differs somewhat from that conventionally used in TST in that the $\Delta G^{\ddagger}$ here is a true equilibrium constant; i.e., we have not extracted the reaction coordinate motion from $\Delta G^{\ddagger}$, and thus, there is no ($k_B T/h$) factor here.
(24) One exception to this statement is the short note published during the earliest stages of the present work. Chapman, C. F.; Marrone, T. J.; Moog, R. S.; Maroncelli, M. In *Ultrafast Phenomena VIII*; Martin, J.-L., Migus, A., Mourou, G. A., Zewail, A. H., Eds.; (Springer-Verlag: Berlin, 1993; p 624.
(25) Jorgensen, W. L. *BOSS*, Version 3.5; Yale University: New Haven, CT, 1994.
(26) Under these conditions *tert*-butyl alcohol is actually a solid (mp, 25.5 °C); however, no behavior signaling an incipient phase transition was observed in this case.
(27) See, for example, the following. *Computer Simulation of Liquids;* Allen, M. P., Tildesley, D. J., Eds.; Oxford, 1987.
(28) This $w(R_{NH}, R_{HO})$ function, which is somewhat unusual, was arrived at by trial and error. The more commonly used harmonic constraint potentials were not as useful for our purposes.
(29) Kumar, P. V.; Maroncelli, M. *J. Chem. Phys.* **1995**, *103*, 3038.
(30) The semiempirical calculations performed with the following program. *AMPAC*, Version 5.0; SemiChem: Shawnee, KS, 1995.
(31) Pranata, J.; Wierschke, S. G.; Jorgensen, W. L. *J. Am. Chem. Soc.* **1991**, *113*, 2810.
(32) Ab initio calculations were performed with the Gaussian94 program. Frisch, M. J.; Trucks, G. W.; Schlegel, H. B.; Gill, P. M. W.; Johnson, B. G.; Robb, M. A.; Cheeseman, J. R.; Keith, T.; Petersson, G. A.; Montgomery, J. A.; Raghavachari, K.; Al-Laham, M. A.; Zakrzewski, V. G.; Ortiz, J. V.; Foresman, J. B.; Cioslowski, J.; Stefanov, B. B.; Nanayakkara, A.; Challacombe, M.; Peng, C. Y.; Ayala, P. Y.; Chen, W.; Wong, M. W.; Andres, J. L.; Replogle, E. S.; Gomperts, R.; Martin, R. L.; Fox, D. J.; Binkley, J. S.; Defrees, D. J.; Baker, J.; Stewart, J. P.; Head-Gordon, M.; Gonzalez, C.; Pople, J. A. *Gaussian 94*, Revision B.1; Gaussian, Inc.: Pittsburgh, PA, 1995. Charges fit according to the Merz−Singh−Kollman scheme, Singh, U. C.; Kollman, P. A. *J. Comput. Chem.* **1984**, *5*, 129. Besler, B. H.; Merz, K. M.; Kollman, P. A. *J. Comput. Chem.* **1990**, *11*, 431.
(33) See the examples and discussion in the following. Reynolds, L.; Gardecki, J. A.; Frankland, S. J. V.; Horng, M. L.; Maroncelli, M. *J. Phys. Chem.* **1996**, *100*, 10337.
(34) We have used MC simulations to compute the association constants for 1:1 complexes between these solutes and a number of complexing partners for which there is dilute solution data available. We find reasonably good agreement using the same solute−solvent potentials employed here. [Mente, S.; Moog, R. S.; Maroncelli, M. Manuscript in preparation.]
(35) These values are from geometry-optimized AM1/CI calculations performed with the AMPAC program[30] using key word "CI=12" specifying use of an CI calculation of 100 microstates formed from selected excitations among the 12 molecular orbitals bracketing the HOMO−LUMO gap.
(36) Reynolds, L. E.; Maroncelli, M. Unpublished results on 1-AC acid−base equilibria.
(37) Jorgensen, W. L.; Madura, J. D.; Swenson, C. J. *J. Am. Chem. Soc.* **1984**, *106*, 6638.
(38) Jorgensen, W. L. *J. Phys. Chem.* **1986**, *90*, 1276.
(39) Jorgensen, W. L.; Chandrasekhar, J.; Madura, J. D.; Impey, R. W.; Klein, M. L. *J. Chem. Phys.* **1983**, *79*, 926.
(40) Gough, C. A.; DeBolt, S. E.; Kollman, P. A. *J. Comput. Chem.* **1992**, *13*, 963.
(41) Fuke, K.; Yoshiuchi, H.; Kaya, K. *J. Phys. Chem.* **1984**, *88*, 5840. Fuke, K.; Yabe, T.; Chiba, N.; Kohida, T.; Kaya, K. *J. Phys. Chem.* **1986**, *90*, 2309.
(42) See, for example, the following. Nakagawa, T.; Kohtani, S.; Itoh, M. *J. Am. Chem. Soc.* **1995**, *117*, 7952 and references therein.
(43) Jeffrey, G. A. *An Introduction to Hydrogen Bonding*; Oxford University Press: New York, 1997.
(44) Chou, P.-T.; Wei, C.-Y.; Chang, C.-P.; Meng-Shin, K. *J. Phys. Chem.* **1995**, *99*, 11994.
(45) Gordon, M. S. *J. Phys. Chem.* **1996**, *100*, 3974.
(46) Herbich, J.; Dobkowski, J.; Thummel, R. P.; Hegde, V.; Waluk, J. *J. Phys. Chem. A* **1997**, *101*, 5839.
(47) Northrup, S. H.; Hynes, J. T. *J. Chem. Phys.* **1980**, *73*, 2700. Hynes, J. T. In *The Theory of Chemical Reactions*; Baer, M., Csizmadia, I. G., Eds.; CRC Press: Boca Raton, FL, 1985; p 171. Northrup, S. H.; Hynes, J. T. *J. Chem. Phys.* **1978**, *69*, 5246.
(48) Northrup, S. H.; Hynes, J. T. *J. Chem. Phys.* **1980**, *73*, 2700 (Appendix C).
(49) This need not be the case. One might have imagined the cyclic form to be a local minimum in the solvation free energy surface, in which case the reactive geometry once formed would persist for some time. However, in none of the systems studied have we found evidence of the cyclic geometry being at a local minimum in free energy.
(50) Pratt, K. C.; Wakeham, W. A. Self-Diffusion in Water and Monohydric Alcohols. *Trans. Faraday Soc. 2* **1977**, *73*, 997.
(51) Matsumoto, M.; Gubbins, K. E. *J. Chem. Phys.* **1990**, *93*, 1981.
(52) Different criteria have been used by other researchers to define hydrogen bonding in pure liquid systems. These have included the use of molecular pair interaction energies or more elaborate geometric criteria. In our case, the use of interaction energies is not possible because we are attempting to differentiate the higher-energy end of many possible hydrogen-bonded configurations rather than just distinguishing between hydrogen-bonded and non-hydrogen-bonded structures. Geometrically, we have considered using, in addition to the two distance parameters, an extra dimension, the angle denoted "χ" (formed by connecting the solute hydrogen active site with the solvent oxygen and the first carbon), which would pick out configurations in which less nuclear rearrangement would be needed if the actual proton shuttling were to occur. However, even by use of the non-Boltzman sampling scheme, it was too difficult to obtain accurate results for $f^{\ddagger}$ using this criterion.
(53) This manner of charge variation was motivated by ab initio calculations, which show that in different alkyl alcohols the H atom charge is nearly constant while the O atom charge and the group to which it is attached account for most of the variations observed.
(54) This feature of the TFE model is disturbing since empirically TFE is found to be a much stronger hydrogen bond donor than methanol. See for example, the following. Abraham, M. H. *Chem. Soc. Rev.* **1993**, *22*, 73. Marcus, Y. *J. Solution Chem.* **1991**, *20*, 929.
(55) We note that these comparisons for water assume the overall reaction time of 830 ps reported by Chapman and Maroncelli.[14] However, there are two time constants observed in the 7AI−water system, this slow time and a much faster time of ∼100 ps, and there is some disagreement in the literature as to which of these two times is associated with the reaction.[14,15] If, instead of this 830 ps, we use the time of 70 ps favored by Petrich and co-workers[15] (ignoring the fact that in their model only a small fraction of molecules are envisioned to react), we would compute a time constant of $\tau_{PT} \approx 50$ fs.
(56) Nakajima, A.; Hirano, M.; Hasumi, R.; Kaya, K.; Watanabe, H.; Carter, C. C.; Williamson, J. M.; Miller, T. L. *J. Phys. Chem. A* **1997**, *101*, 392.
(57) This identification assumes that k_{PT} is activationless, which is implied by the experimental observation that the isotope effect is temperature-independent.[21]
(58) Based on the data in ref 20 over the temperature range 203−323 K. Uncertainties listed here are ±2 standard deviations.
(59) Mente, S.; Maroncelli, M. Work in progress.
(60) Reynolds, L. E.; Maroncelli, M. To be published.